Integrated Effect of Attitude Motion Control and Electronic Stability Control based on 14-DOF Nonlinear Full Vehicle Model

A Dissertation Submitted to the Faculty of the Graduate School of the Gyeongsang National University

By

Edward Youn

In partial fulfillment of the requirements

for the degree

of Master of Science

June, 2016

Dr. Iljoong Youn, Dissertation Supervisor

Acknowledgement

I would like to first express my deep gratitude towards Professor Iljoong Youn for giving me an opportunity to study vehicle dynamics in depth at Gyeongsang National University and for being an outstanding supervisor with his step-by-step guidance to help me reach where I am today. His concept-based teachings not only provided me with strong understanding of my research area, but also encouraged me to become a better researcher overall.

I would like to thank the committee, Professor Gun-Myung Lee and Dr. Rodrigue Tchamna for their precious time spent on carefully evaluating my thesis and offering valuable advices and comments.

I would like to thank my friend, Arshad M. Khan, for keeping me company in System Control Lab and helping me in completing this thesis with countless useful discussions and thoughts based on his many years of field experience.

My thanks also go to the staffs at the department along with the members of System Control Lab for creating such pleasant environment for research and studies.

Finally, my greatest appreciation goes to my family, those I love, and the Lord who always help me stay humble, motivate me during times of hardship, and warm my heart with unconditional love.

Table of Contents

List of Figures and Tables

Abstract

Integrated Effect of Attitude Motion Control and Electronic Stability Control based on 14-DOF Nonlinear Full Vehicle Model

Edward Youn
Department of Mechanical and Aerospace Engineering
Graduate School, Gyeongsang National University
Supervised By
Professor Iljoong Youn

The aim of this thesis is to analyze the advantages of the electronic stability controller (ESC) and the attitude motion controller (AMC), and to study the synergistic effect of the two controllers on comprehensively improving vehicle safety, handling capability, and lateral ride comfort. The ESC, which uses rear braking torques to enhance the vehicle's response to the desired yaw rate while keeping the sideslip under control, is designed based on a 7-degrees-of-freedom (DOF) full vehicle model. This 7-DOF model for ESC takes into account the vehicle's longitudinal, lateral, and yawing motions, along with the rotational velocity of each tire. The AMC, which uses active suspension forces to control the vehicle's attitude motion consisting of roll and pitch motions, is designed based on another 7-DOF linear full vehicle. This 7-DOF linear model for AMC takes into account the vehicle's vertical,

rolling and pitching motions, along with the vertical motion of each tire.

Although the AMC does not have direct influence on the horizontal motions of the vehicle, the two controllers are closely related to each other through the tire models which calculate the longitudinal and lateral tire forces based on the vertical tire force. The AMC indirectly helps improving ESC's performance by balancing out the vertical tire force distribution.

The two controllers are integrated and applied to a 14-DOF nonlinear full vehicle model which takes into account all of the motions listed for both 7-DOF models. The effectiveness of the individual controllers and the integrated controller is thoroughly evaluated via simulations in various conditions.

초록

14 자유도 비선형 차량 모델을 이용한 주행 안정성 제어와 자세 제어의 통합 효과

윤선용
경상대학교 기계항공공학부 기계공학과
지도교수: 윤일중

본 논문은 주행 안정성 제어 시스템 (Electronic Stability Control, ESC)와 자세 제어 시스템 (Attitude Motion Control, AMC)의 이점을 분석하고 두 제어방식의 통합효과가 자동차의 안정성, 기동성, 승차감에 미치는 영향에 초점을 둔다.
뒷바퀴의 토크를 이용해 차체의 요잉각 속도와 횡활각을 제어하는 ESC는 차체의 평면속도와 요잉각 속도 및 각 바퀴의 회전속도를 고려하는 7 자유도 차량모델을 기반으로 설계되었다. 이에 비해 능동 현가장치를 사용하여 차체의 롤각(Roll angle)과 피치각(Pitch angle)을 제어하는 AMC는 차체의 수직속도, 롤각, 피치각 및 각 바퀴의 수직속도를 고려한 7 자유도 선형 차량모델을 기반으로 설계되었다.
비록 AMC는 ESC처럼 차체의 평면운동에 직접적인 영향을 미치지는 않지만 AMC와 ESC는 바퀴 수직력과 평면 마찰력의 관계식을 통해 서로 긴밀히 연관되어있다. AMC는 각 바퀴의 수직력을 균일하게 분배하여 결과적으로 평면마찰력의 균형을 잡음으로써 ESC의 성능을 간접적으로 향상시킨다.
AMC와 ESC의 통합제어 시스템은 앞서 언급된 두 7자유도 모델의 모든 운동을 고려한 14 자유도 비선형모델에 적용되어 다양한 조건 하 시뮬레이션을 통해 그 성능이 비교 분석 및 평가되었다.

1. INTRODUCTION

With user needs and development in technology, modern ground vehicles are becoming more complex means of transportation with higher degrees of ride comfort and safety. Two of the techniques to improve vehicle safety, handling, and ride comfort are electronic stability control (ESC) [1] and active suspension control. Attitude motion control (AMC) is a type of active suspension control that uses a hydraulic actuator at each suspension to create desired force upon the car body [2]. Unlike passive suspension systems, the AMC can both add and dissipate energy from the system. With the AMC, the force actuator can apply force independent of the relative displacement or velocity across the suspension. The AMC results in a better compromise between ride comfort and vehicle stability as compared to a passive system [4, 5]. Compared to other active suspension systems, the AMC has the added advantage of controlling the attitude of a vehicle, which means it can react properly to the changing pitching and rolling angles due to braking, acceleration, or centrifugal forces much like as done in [6]. More examples on full-vehicle active safety control systems on global chassis control are given in [2, 7].

ESC, as an extension of Anti-lock Braking System, provides unequal braking torques to the vehicle's wheels in order to create necessary yaw moment to control the yaw rate [3], which in turn enables the vehicle to follow the driver's intended direction. However, because of its dependency on the vehicle velocity, sideslip angle, and the steering wheel angle, ESC has a number of limitations. For instance, the conventional ESC relies solely on the braking forces of rear tire in order to generate necessary yaw moment, and a major drawback of the result is heavy reduction in vehicle speed. This problem was resolved by introducing an improved ESC with added torque transferring capability. By enabling the ESC to accelerate one wheel while decelerating the other using techniques such as torque vectoring or all-wheel-drive, the ESC minimizes the longitudinal speed reduction and generates equally effective yaw moment.

Another limitation of the ESC is that the only factor that ESC can utilize to create controlled yaw moment is the traction between each tire and the ground. If the wheels on one side of the vehicle have much less traction than the ones on the other side, ESC may not work to its full potential because the wheel with less traction may not be able to create enough torque provided that the wheel's rotational velocity has an upper boundary. Integration of AMC with ESC mitigates this problem by evenly distributing vertical forces of the four tires. During cornering, accelerating, or braking, the uncontrolled passive vehicle tends to lean towards the direction of the body force such as centrifugal force. This creates uneven distribution of vertical tire forces; the tires on one side have much greater traction than the ones on the other side. The attitude controller developed for AMC calculates active suspension forces required to make the vehicle tilt towards the opposite direction of the body force, thus shifting the mass center, which in turn evens out the ground forces acting upon tires and reduces the acceleration acting on the car body, resulting in more reliable ESC.

The effects of integration of ESC and AMC are evaluated through simulations run on 14-DOF nonlinear full vehicle model at various vehicle speeds. Three types of steering conditions are considered for simulation inputs: over-steering, under-steering, and neutral-steering. An over-steering condition refers to a vehicle highly sensitive to the steering angle. This is achieved by placing the center of gravity closer to the front than the rear. By doing so, bigger vertical force will be provided to the front tires, generating bigger longitudinal and lateral forces in the front than back. As a result, the vehicle will show more sensitive response to the changing steering angle in the front. On the other hand, an under-steering condition is achieved by placing the center of gravity closer to the rear than the front, resulting in the vehicle less sensitive to the steering angle. Generally, an over-steering vehicle is perceived as less stable, and an under-steering vehicle is more stable but sluggish. Although neutral-steering conditions are considered to be ideal for the steering wheel response, but the conventional ground vehicles are designed to be varying degrees of under-steering for safety issues because neutral-steering vehicles can lose stability easily. The proposed integrated controller's performance effectiveness is decided by how well it makes an over-steering vehicle behave more like a neutral-steering vehicle.

This thesis is organized in four main sections. In section 2, the vehicle models used in this paper are explained. In section 3, controller design techniques are discussed. The simulation and analysis are carried out in section 4 and conclusion is presented in section 5.

2. VEHICLE MODELS

Three different full vehicle models are used in this study for the control designs and simulation purposes. The design of ESC utilizes a 7-DOF nonlinear model which takes into account the longitudinal, lateral, and yaw motions of the vehicle chassis, and the rotational motion of each wheel. The design of AMC utilizes another 7-DOF linear model which takes into account the vertical, roll, and pitch motions of the vehicle chassis in addition to the vertical motion of each wheel. The integration of the two controllers is then applied to and simulated on a 14-DOF nonlinear model which takes into account every degree mentioned in the first two full vehicle models. The application of 14-DOF nonlinear model allows taking into consideration nonlinear load transfer and coupling effects between the vehicle suspension and the handling dynamics.

2.1. 7-DOF NONLINEAR MODEL FOR ESC

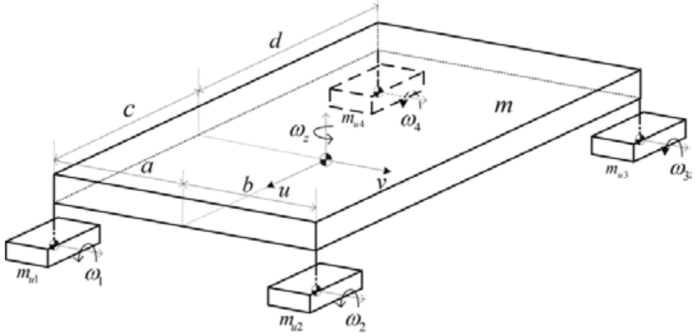

Figure 1: The overall schematic for the 7-DOF model for ESC

A 7-DOF full vehicle model is used to study differential braking-based yaw stability control system also known as ESC. **Figure 1** and **Figure 2** illustrate the schematics for the 7-DOF model used for ESC. This model includes 3-DOF as lateral (u), longitudinal (v) and yaw (ω_z) motions of the car body, in addition to the 4-DOF as angular velocities of the four wheels (ω_i) where the subscript i denotes numbers 1 through 4, which represent right front, left front, left rear, and right rear wheels respectively. The subscript i will be used in the same manner throughout the paper.

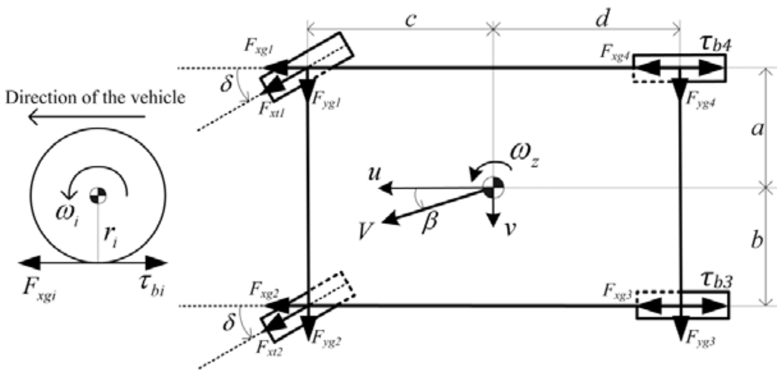

Figure 2: The schematics of the tire model and upper view of the 7-DOF model

$$m_T\left(\dot{u}-\omega_z v\right)=\sum F_{xg_i} \tag{1}$$

$$m_T\left(\dot{v}+\omega_z u\right)=\sum F_{yg_i} \tag{2}$$

$$J_z\dot{\omega}_z = a\left(F_{xg1}+F_{xg4}\right)-b\left(F_{xg2}+F_{xg3}\right)+c\left(F_{yg1}+F_{yg2}\right)-d\left(F_{yg3}+F_{yg4}\right) \tag{3}$$

where J_z denotes the yaw inertia of the car body, and m_T the summation of m and Σm_{ui}. The equations of F_{xgi} and F_{ygi} are given by:

$$\begin{aligned} F_{xgi} &= F_{xti}\cos\delta_i - F_{yti}\sin\delta_i \\ F_{ygi} &= F_{xti}\sin\delta_i + F_{yti}\cos\delta_i \end{aligned} \tag{4}$$

The δ_i denotes the steering angle of each wheel, and this thesis assumes δ_i = 0 for i = {3, 4}. Additionally, the dynamic equation for each wheel is:

$$J_{wi}\dot{\omega}_i = -F_{xti} r_i + \tau_{bi} \tag{5}$$

where J_{wi}, r_i, and τ_{bi} denote the rotational inertia, instantaneous radius, and ESC braking torque of each wheel, respectively. The method to obtain F_{xti} and F_{yti} is discussed in Section 2.3.

2.2. 7-DOF LINEAR MODEL FOR AMC

A 7-DOF linear full car model is used to design AMC based on active suspension control. Unlike the former model, this model ignores u, v, ω_z, and the rotational velocity of each wheel. Instead, the 7-DOF in this model includes pitch (Θ), roll (ϕ), heave (z_c) motions of the car body, in addition to vertical velocity (z_i) of each of four wheels. **Figure 3** illustrates the schematics for the 7-DOF model used for AMC.

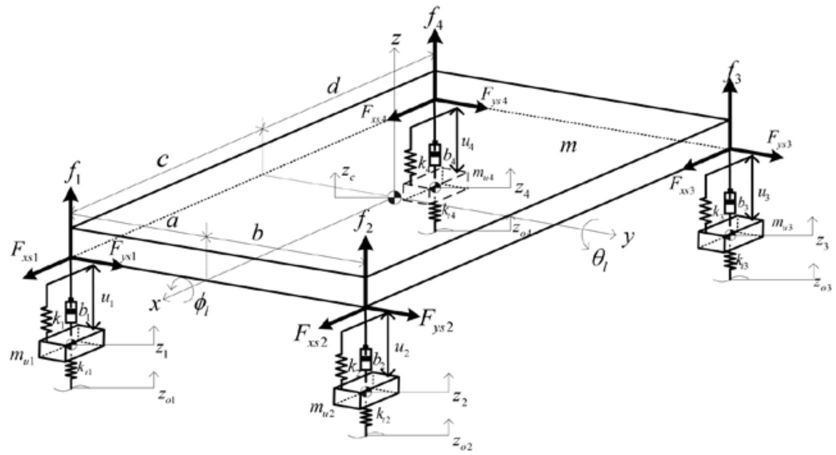

Figure 3: The overall schematic for the 7-DOF linear model for AMC

The dynamic equations for the car body model used in AMC design are:

$$m\ddot{z}_c = \sum_{i=1}^{4} f_i \tag{6}$$

$$J_x\ddot{\phi}_l = h_r\sum_{i=1}^{4}\left(-F_{ysi}\right) - (f_1 + f_4)a + (f_2 + f_3)b \tag{7}$$

$$J_y\ddot{\theta}_l = h_p\sum_{i=1}^{4}F_{xsi} - (f_1 + f_2)c + (f_3 + f_4)d \tag{8}$$

$$m_{ui}\ddot{z}_i = k_{ti}z_{ti} - f_i \tag{9}$$

Notice that the value z_{ti} is the tire deflection of each wheel and can be summarized as:

$$z_{ti} = z_{oi} - z_{ui} \tag{10}$$

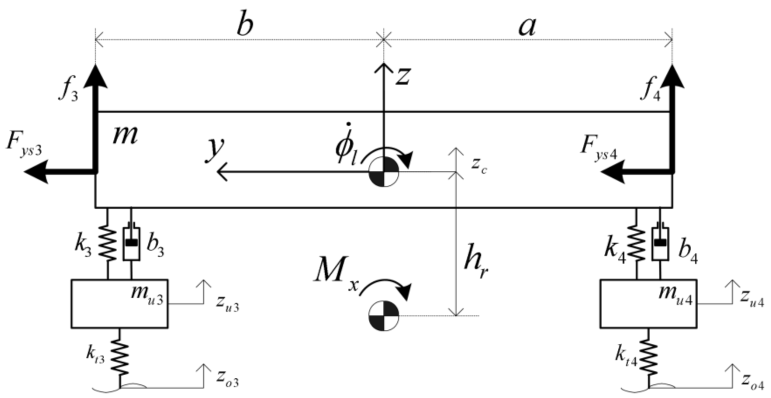

Figure 4: The rear view of the 7-DOF linear vehicle model for AMC

The summations of F_{xsi} and F_{ysi} in equations (7) and (8) are the total longitudinal and lateral forces acting on car body. Since the model is unable to generate these forces independently, the forces are directly imported from the nonlinear model described in the next section. **Figure 4** illustrates the rear view of the 7-DOF linear vehicle model for AMC. The distance of the roll center of the vehicle to c.g. is denoted by h_r and is multiplied by the summations of forces to calculate rolling and pitching momentums generated by the ground forces. Suspension forces of car body, f_i, are generated by the addition of actuators to the suspension system. Adding the control force (u_i) with spring and dumper can produce upward and downward forces, the equations for these forces are:

$$\begin{aligned} f_1 &= k_1 z_{s1} + b_1 \dot{z}_{s1} + u_1 \\ f_2 &= k_2 z_{s2} + b_2 \dot{z}_{s2} + u_2 \\ f_3 &= k_3 z_{s3} + b_3 \dot{z}_{s3} + u_3 \\ f_4 &= k_4 z_{s4} + b_4 \dot{z}_{s4} + u_4 \end{aligned} \tag{11}$$

where z_{si} is the deflection value of each suspension, and the suspension deflections can be summarized as:

$$\begin{aligned} z_{s1} &= z_{u1} - z_c + c\theta_l + a\phi_l \\ z_{s2} &= z_{u2} - z_c + c\theta_l - b\phi_l \\ z_{s3} &= z_{u3} - z_c - d\theta_l - b\phi_l \\ z_{s4} &= z_{u4} - z_c - d\theta_l + a\phi_l \end{aligned} \tag{12}$$

where z_{ui} denotes the vertical displacement of c.g. of each tire. Finally, for the purpose of simulating the linear model, total 17 states are defined as:

$$\mathbf{x_l} = \left[\dot{z}_c, \theta_l, \phi_l, \dot{\theta}_l, \dot{\phi}_l, z_{s1}, z_{s2}, z_{s3}, z_{s4}, z_{t1}, z_{t2}, z_{t3}, z_{t4}, \dot{z}_{u1}, \dot{z}_{u2}, \dot{z}_{u3}, \dot{z}_{u4} \right]^{\mathbf{T}} \tag{13}$$

2.3. 14-DOF NONLINEAR MODEL

The 7-DOF models are sufficient to test the ESC and AMC separately. However, in order to evaluate the performance of the integration of the two controllers, a more complex model is required. Notice that the two models do not have any common degree of freedom. 7-DOF from each model will be put together to design a 14-DOF nonlinear model. **Figure 5** illustrates the schematics of the 14-DOF nonlinear full car model used in investigating the vehicle side slip angle and yaw rate in response to steering angle, active suspension, and brake torque inputs. The nonlinear passive vehicle model as discussed in [2] consists of 6-DOF at the mass centre of the vehicle body and 2-DOF at each of the four wheels. The 6-DOF represent the vehicle body's longitudinal, lateral, and vertical motions in addition to roll, pitch, and yaw motions in *x*, *y*, and *z* directions of the body-fixed coordinate. The 2-DOF at each of the four wheels consists of vertical and rotational motions of each wheel.

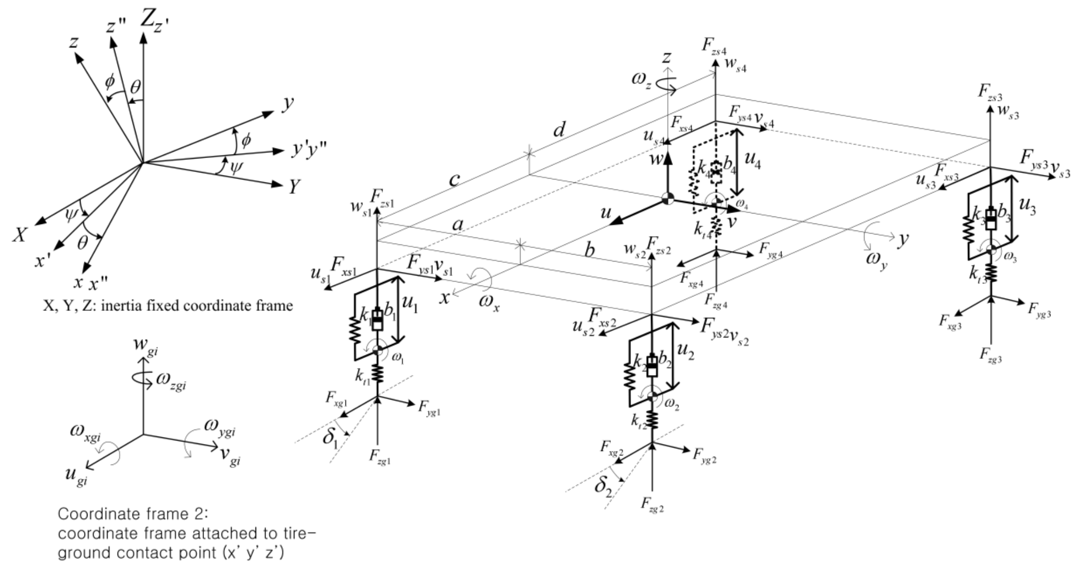

Figure 5: The overall schematic for the 14-DOF nonlinear full vehicle model

The set of dynamic equations for the 14-DOF nonlinear model follows:

$$m\left(\dot{u}+\omega_y w-\omega_z v\right)=\sum F_{xs_i}+mg\sin\theta \tag{14}$$

$$m\left(\dot{v}+\omega_z u-\omega_x w\right)=\sum F_{ys_i}-mg\sin\phi\cos\theta \tag{15}$$

$$m\left(\dot{w}+\omega_x v-\omega_y u\right)=\sum\left(F_{zs_i}+F_{dz_i}\right)-mg\cos\phi\cos\theta \tag{16}$$

$$J_x\dot{\omega}_x=\sum\mathbf{M}_{xi}-a\left(F_{zs1}+F_{zs4}\right)+b\left(F_{zs2}+F_{zs3}\right) \tag{17}$$

$$J_y\dot{\omega}_y=\sum\mathbf{M}_{yi}-c\left(F_{zs1}+F_{zs2}\right)+d\left(F_{zs3}+F_{zs4}\right) \tag{18}$$

$$J_z\dot{\omega}_z=\sum\mathbf{M}_{zi}+a\left(F_{xs1}+F_{xs4}\right)-b\left(F_{xs2}+F_{xs3}\right)+c\left(F_{ys1}+F_{ys2}\right)-d\left(F_{ys3}+F_{ys4}\right) \tag{19}$$

where $\dot{u}$, $\dot{v}$ and $\dot{w}$ are the longitudinal, lateral, and vertical accelerations at the c.g. of the vehicle in body fixed coordinate, respectively. Similarly, $\dot{\omega}_x$, $\dot{\omega}_y$ and $\dot{\omega}_z$ are the roll, pitch, and yaw angular accelerations, respectively. The remaining 8-DOF consists of 2-DOF representing vertical and rotational motion at each wheel in the following form:

$$m_{ui}\left(\dot{w}_{ui}+\omega_x v_{ui}-\omega_y u_{ui}\right)=F_{zgsi}-m_{ui}g\cos\theta\cos\phi-F_{zsi}-F_{dzi} \tag{20}$$

$$J_i\dot{\omega}_i=-F_{xti}r_i+\tau_b \tag{21}$$

where w_{ui} and ω_i are vertical acceleration and angular acceleration of each wheel. The cardan angles Θ, ϕ, and ψ can be derived from the following differential equations:

$$\dot{\theta} = \omega_y \cos\phi - \omega_z \sin\phi \tag{22}$$

$$\dot{\phi} = \omega_x + \omega_y \sin\phi \tan\theta + \omega_z \tan\theta \cos\phi \tag{23}$$

$$\dot{\psi} = \omega_y \frac{\sin\phi}{\cos\theta} + \omega_z \frac{\cos\phi}{\cos\theta} \tag{24}$$

Finally, the list of 25 states used in deriving the differential equations of the nonlinear model follows:

$$\begin{aligned}\mathbf{x_n} = \big[& u, v, w, \theta, \phi, \psi, \omega_y, \omega_x, \omega_z, \omega_1, \omega_2, \omega_3, \omega_4, \\ & x_{s1}, x_{s2}, x_{s3}, x_{s4}, x_{t1}, x_{t2}, x_{t3}, x_{t4}, w_{u1}, w_{u2}, w_{u3}, w_{u4} \big]^{\mathbf{T}}\end{aligned} \tag{25}$$

where x_{s1-4} and x_{t1-4} denote the suspension and tire deflections of each wheel, respectively. More detailed list of equations of the 14-DOF nonlinear model will be given in Appendix A.

Two different tire models are utilized in this study as the means to acquire the tire forces, F_{xti} and F_{yti}. The linear tire model simply calculates the forces as the product of the cornering (or longitudinal) tire stiffness and the sideslip angle (or longitudinal slip ratio), whereas the pacejka tire model plugs in the experimentally chosen constants into Pacejka Magic Formula. More comprehensive comparison between the tire models are made in the Simulations and Analysis section.

2.3.1. Linear Tire Model

An advantage of the linear tire model is that it uses simple linear equations.

However, with these simple equations come obvious limitations. The tire forces are linearly correlated to the tire slip ratio and sideslip angle, and are only accurate in the small range around zero slip conditions. If slip value exceeds a certain threshold, the linear tire model will not generate accurate results.

The tire forces are calculated in the following equations:

$$F_{xti} = \frac{F_{zgi}}{F_{zgi,static}} C_{ti} \alpha_{xi} \tag{26}$$

$$F_{yti} = -\frac{F_{zgi}}{F_{zgi,static}} C_{\alpha i} \alpha_{yi} \tag{27}$$

where C_{ti}, C_{ai}, a_{xi}, and a_{yi} are longitudinal stiffness, cornering stiffness, longitudinal slip ratio, and sideslip angle of the tire, respectively.

As described in [9], the longitudinal slip ratio and sideslip angle of the tire are given as:

$$\alpha_{xi} = \frac{r_i \omega_i - u_{ui}}{\max\left(r_i \omega_i, u_{ui}\right)} \tag{28}$$

$$\alpha_{yi} = \tan^{-1}\left(\frac{v_{gi}}{u_{gi}}\right) - \delta_i \tag{29}$$

Division of vertical tire force, F_{zgi}, by the static vertical force, $F_{zgi,static}$, is necessary in order to take into account the vertical force distribution of the four wheels depending on the location of center of gravity of the vehicle.

They are calculated as:

$$F_{zgi} = k_{ti} x_{ti} \tag{30}$$

$$F_{zg1,static} = \frac{bd}{(a+b)(c+d)} mg + m_{u1} g \tag{31}$$

$$F_{zg2,static} = \frac{ad}{(a+b)(c+d)} mg + m_{u2} g \tag{32}$$

$$F_{zg3,static} = \frac{ac}{(a+b)(c+d)} mg + m_{u3} g \tag{33}$$

$$F_{zg4,static} = \frac{bc}{(a+b)(c+d)} mg + m_{u4} g \tag{34}$$

where k_{ti} is the spring constant of each wheel.

2.3.2. Pacejka Tire Model

Because of the linear tire model's inevitable limitations, pacejka tire model is implemented according to [10]. In comparison with the linear tire model, the pacejka model does a much better job in mimicking the real tire's behavior. The pacejka model shows similar behavior as the linear tire model up to a certain point, and then the tire forces show a gradual decrease much like in a real life scenario. The pacejka tire model takes F_{zgi} and a_{xi} (or a_{yi}) given in equations (28) and (29) as inputs. Whether calculating the longitudinal or lateral tire force, the pacejka model has its base equation as the following:

$$F_j(F_{zgi},\alpha_{ji}) = D\sin\left\{C\tan^{-1}\left(B_x\right)\right\} + V \tag{35}$$

where the subscript j denotes the x or y directions of force, and

$$B_x = B\left(1-E\right)\left(\alpha_{ji}+H\right) + E\left[\tan^{-1}\left\{B\left(\alpha_{ji}+H\right)\right\}\right] \tag{36}$$

The value of a_{ji} is either a_{xi} or a_{yi}. Depending on the values of B, C, D, E, H, V, and x the output of the equation can resemble longitudinal force, lateral force, or self-aligning torque (M_z) of the tire. The M_z is assumed to be zero in this study because steering angles of the wheels are arbitrarily set, uninfluenced by M_z. The effect of M_z is negligible in any simulations.

The factor B is called the stiffness factor because it influences the slope of the output at the origin. The equation of B follows:

$$B = \begin{cases} \dfrac{a_3 F_{zgi}{}^2 + a_4 F_{zgi}}{CDe^{a_5 F_{zgi}}} & \text{for } F_{xti} \\ a_3 \sin\left\{a_4 \tan^{-1}\left(a_5 F_{zgi}\right)\right\} \dfrac{1 - a_{12}\left|\gamma\right|}{CD} & \text{for } F_{yti} \end{cases} \tag{37}$$

where the tire camber angle (γ) is assumed to be zero in this study. The constants a_j appear in the calculations of other factors as well, and are used to fine tune the final output of the Magic Formula.

The factor C is called shape factor because influences the limits of the range of the argument of the sine function and it is simply defined as:

$$C = a_0 \tag{38}$$

Since the factor D determines the peak amplitude of the output, it is called the peak factor, and is defined as:

$$D = a_1 F_{zgi}^{\ 2} + a_2 F_{zgi} \tag{39}$$

The amplitude of the peak value is determined by D, but at what time it occurs is determined by E, which is therefore called the curvature factor. The bigger the value of E, the further away the peak value is from the origin. The equation for the curvature factor is as the following:

$$E = a_6 F_{zgi}^{\ 2} + a_7 F_{zgi} + a_8 \tag{40}$$

Finally, the vertical and horizontal shifts of the tire force are determined by V and H, but, as shown in the following equations, they are both assumed zero because the camber angle is zero.

$$V = \begin{cases} 0 & \text{for } F_{xti} \\ a_{10} F_{zgi}^{\ 2} + a_{11} F_{zgi} |\gamma| & \text{for } F_{yti} \end{cases} \tag{41}$$

$$H = \begin{cases} 0 & \text{for } F_{xti} \\ a_9 |\gamma| & \text{for } F_{yti} \end{cases} \tag{42}$$

2.3.3. Combined Pacejka Tire Model

When braking maneuver and cornering maneuver are performed separately, the pacejka tire model above gives satisfying results for the longitudinal and lateral tire friction forces. However, when braking and cornering are performed simultaneously, as in this study, calculating the longitudinal and lateral forces separately will result in error because the two forces are closely coupled together. Therefore, adjustments in the tire force equations are required.

The vectors and values required for this method are illustrated in Figure 6:

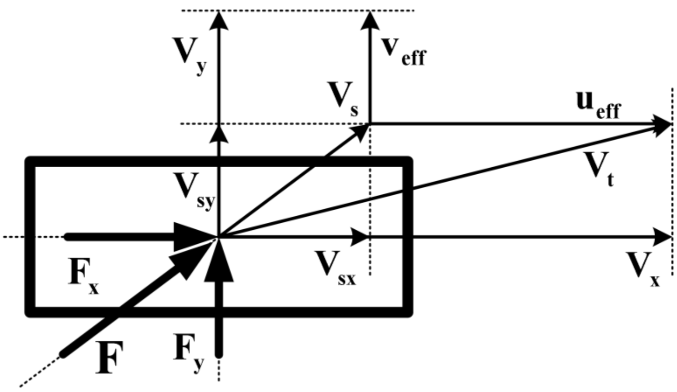

Figure 6: The top view of the tire schematics for combined pacejka model

V_x is a product of the instantaneous radius and the rotational velocity of the tire which represents the expected longitudinal velocity. u_{eff} is the effective longitudinal velocity of the tire. The difference between the expected and the effective longitudinal velocities is the longitudinal slip velocity, V_{sx}. Likewise, the difference between the expected (V_y) and the effective (v_{eff}) lateral velocities is the lateral slip velocity, V_{sy}. However, the value of expected lateral velocity is zero, thus the value of V_{sx} is equal to v_{eff} in the opposite direction.

$$\begin{aligned} V_x &= r_i \omega_i \\ V_y &= 0 \end{aligned} \tag{43}$$

$$\begin{aligned} V_{sx} &= V_x - u_{eff} \\ V_{sy} &= V_y - v_{eff} = -v_{eff} \end{aligned} \tag{44}$$

In this method, new theoretical slip value and its components are introduced as the following:

$$\begin{aligned} \varphi_x &= \frac{V_{sx}}{u_{eff}} \\ \varphi_y &= \frac{V_{sy}}{u_{eff}} \\ \varphi &= \sqrt{{\varphi_x}^2 + {\varphi_y}^2} \end{aligned} \tag{45}$$

Because the new theoretical slip vector has the same direction as the slip speed vector $\mathbf{V_s}$, the following holds true:

$$\begin{aligned} \mathbf{F} &= \frac{\vec{\varphi}}{\varphi} \mathrm{F}(\varphi) \\ \mathbf{F_x} &= \frac{\varphi_x}{\varphi} \mathrm{F_x}(\varphi) \\ \mathbf{F_y} &= \frac{\varphi_y}{\varphi} \mathrm{F_y}(\varphi) \end{aligned} \tag{46}$$

where $\mathrm{F_j}(\phi)$ is a pacejka model described in Equation (35). More detailed explanation is available in the reference [10].

3. CONTROL DESIGN

In the previous section, three types of full car models are introduced: 7-DOF nonlinear model for ESC, 7-DOF linear model for AMC, and 14-DOF nonlinear model for the integration of the controllers. For ESC, a sliding mode control technique is used to calculate control braking torques to make the vehicle follow the desired yaw rate and sideslip angle. On the other hand, for AMC, an optimal linear attitude controller with tracking control technique is used to calculate the desired control active suspension forces to make the vehicle follow the desired roll and pitch angles. In this section, the implementation of each controller will be reviewed in detail.

3.1. ELECTRONIC STABILITY CONTROL

The main goal of a vehicle stability control system is to assist the vehicle to follow the trajectory intended by the driver by preventing the vehicle from spinning or drifting out. There are various types of vehicle stability controls including anti-lock braking system, steer-by-wire system, and active torque distribution systems. As an extension of anti-lock braking system, the ESC adjusts the vehicle's yaw rate by providing extra braking torque to a wheel which in turn creates necessary yaw moment to keep the vehicle on track.

This research assumes the vehicle to be a four-wheeled vehicle with a rear differential. The critical drawback of the conventional ESC as opposed to steering wheel controller is that the control forces can only provide braking torque, resulting in inevitable decrease in vehicle speed. The conventional rear-differential drive vehicle cannot distribute torque efficiently. However, this speed reduction can be mitigated if the ESC has full control over the torque distribution using techniques such as torque distribution or all-wheel motor drive; the wheels can now not only brake, but also accelerate. By splitting the required control force of the inner wheel and feeding it as an acceleration torque to the outer wheel, the controller can generate virtually the same yaw moment with much less decrease in the vehicle speed. More on this is discussed in the later sections.

3.1.1. Conventional ESC

The sliding surface for the controller is defined as:

$$s = \rho_{yaw}\left(\omega_z - \omega_{zd}\right) + \rho_s\left(\beta - \beta_d\right) \tag{47}$$

where ω_{zd}, β, and β_d are desired yaw rate, sideslip angle, and desired sideslip angle at the c.g. of vehicle. ρ_{yaw} and ρ_s are design coefficients for the yaw rate and sideslip angle. The desired yaw rate can be calculated by considering the longitudinal velocity, total length and mass of the vehicle, and the cornering stiffness as given in [9]:

$$\omega_{zd} = \frac{u}{(c+d) + \dfrac{m_T(d-c)}{2(c+d)C_\alpha}u^2}\delta \tag{48}$$

There is a debate on whether the following the calculated desired sideslip angle is significant in achieving a stable maneuver, but this study assumes that β_d = 0 is for the best of interests. The calculation of the theoretical desired sideslip angle will be presented later this section, but it will not be used in the implementation of the ESC.

Differentiation of the sliding surface with $\beta_d = 0$ results in:

$$\dot{s} = \rho_{yaw}\left(\dot{\omega}_z - \dot{\omega}_{zd}\right) + \rho_s \dot{\beta} \tag{49}$$

For the sliding surface to reach zero asymptotically, the dynamics should conform to the following equation:

$$\dot{s} = -K_{ESC} s \tag{50}$$

Replacing s and $\dot{s}$ with equations (47) and (49) results in the following:

$$\rho_{yaw}\dot{\omega}_z + \rho_s \dot{\beta} = \rho_{yaw}\dot{\omega}_{zd} - K_{ESC}\left(\rho_{yaw}\left(\omega_z - \omega_{zd}\right) + \rho_s \beta\right) \tag{51}$$

where K_{ESC} is tuned to control overall effectiveness of ESC. β and $\dot{\beta}$ can be calculated from following equations:

$$\beta = \tan^{-1}\left(\frac{v}{u}\right) \tag{52}$$

$$\dot{\beta} = \left(1 + \tan^2(\beta)\right)^{-1}\left(\frac{\dot{v}}{u} - \frac{\dot{u}}{v}\tan(\beta)\right) \tag{53}$$

The expressions for the longitudinal, lateral, and yaw accelerations of 7-DOF model can be obtained from equations (1), (2), and (3) as the following:

$$\dot{u} = \frac{\sum F_{xg_i}}{m_T} + \omega_z v \tag{54}$$

$$\dot{v} = \frac{\sum F_{yg_i}}{m_T} - \omega_z u \tag{55}$$

$$\dot{\omega}_z = \frac{a\left(F_{xg1} + F_{xg4}\right) - b\left(F_{xg2} + F_{xg3}\right) + c\left(F_{yg1} + F_{yg2}\right) - d\left(F_{yg3} + F_{yg4}\right)}{J_z} \tag{56}$$

Via substitution into equation (53), $\dot{\beta}$ can be written as

$$\dot{\beta} = \frac{\sum_{i=1}^{4} F_{ygi} u - \sum_{i=1}^{4} F_{xgi} v}{m_T \left(u^2 + v^2\right)} - \omega_z \tag{57}$$

By using the relationship between ground forces (F_{xgi}, F_{ygi}) and tire forces (F_{xti}, F_{yti}) given in equation (4), and by substituting $\dot{\omega}_z$ and $\dot{\beta}$, the equation (51) can be reorganized in the following way:

$$\sum_{i=1}^{4} \kappa_{Fxti} F_{xti} + \sum_{i=1}^{4} \kappa_{Fyti} F_{yti} - \rho_s \omega_z = \rho_{yaw} \dot{\omega}_{zd} - K_{ESC} \left(\rho_{yaw}\left(\omega_z - \omega_{zd}\right) + \rho_s \beta\right) \tag{58}$$

$$\sum_{i=1}^{i=4} \kappa_{F_{xti}} F_{xti} = \underbrace{\rho_{yaw} \dot{\omega}_{zd} - K_{ESC} \left(\rho_{yaw}\left(\omega_z - \omega_{zd}\right) + \rho_s \beta\right)}_{\chi_1} - \underbrace{\left(\sum_{i=1}^{4} \kappa_{Fyti} F_{yti} - \rho_s \omega_z\right)}_{\chi_2} \tag{59}$$

Finally substituting F_{xti} with the relationship given in Equation (5):

$$\sum_{i=1}^{4}\kappa_{Fxti}r_i^{-1}\tau_{bi}-\sum_{i=1}^{4}\kappa_{Fxti}r_i^{-1}\dot{\omega}_i J_i=\chi_1-\chi_2 \tag{60}$$

$$\sum_{i=1}^{4}\kappa_{Fxti}r_i^{-1}\tau_{bi}=\chi_1-\chi_2+\underbrace{\sum_{i=1}^{4}\kappa_{Fxti}r_i^{-1}\dot{\omega}_i J_i}_{\chi_3} \tag{61}$$

where κ_{Fxti} and κ_{Fyti} are defined as the following:

$$\begin{aligned}
\kappa_{Fxt1}&=\cos\delta_1\left(\frac{a\rho_{yaw}}{J_z}-\frac{\rho_s v}{m_T\left(u^2+v^2\right)}\right)+\sin\delta_1\left(\frac{c\rho_{yaw}}{J_z}+\frac{\rho_s u}{m_T\left(u^2+v^2\right)}\right)\\
\kappa_{Fxt2}&=\cos\delta_2\left(\frac{-b\rho_{yaw}}{J_z}-\frac{\rho_s v}{m_T\left(u^2+v^2\right)}\right)+\sin\delta_2\left(\frac{c\rho_{yaw}}{J_z}+\frac{\rho_s u}{m_T\left(u^2+v^2\right)}\right)\\
\kappa_{Fxt3}&=\frac{-b\rho_{yaw}}{J_z}-\frac{\rho_s v}{m_T\left(u^2+v^2\right)}\\
\kappa_{Fxt4}&=\frac{a\rho_{yaw}}{J_z}-\frac{\rho_s v}{m_T\left(u^2+v^2\right)}\\
\kappa_{Fyt1}&=\cos\delta\left(\frac{c\rho_{yaw}}{J_z}+\frac{\rho_s u}{m_T\left(u^2+v^2\right)}\right)+\sin\delta_1\left(\frac{-a\rho_{yaw}}{J_z}+\frac{\rho_s v}{m_T\left(u^2+v^2\right)}\right)\\
\kappa_{Fyt2}&=\cos\delta_2\left(\frac{c\rho_{yaw}}{J_z}+\frac{\rho_s u}{m_T\left(u^2+v^2\right)}\right)+\sin\delta_2\left(\frac{b\rho_{yaw}}{J_z}+\frac{\rho_s v}{m_T\left(u^2+v^2\right)}\right)\\
\kappa_{Fyt3}&=\frac{-d\rho_{yaw}}{J_z}+\frac{\rho_s u}{m_T\left(u^2+v^2\right)}\\
\kappa_{Fyt4}&=\frac{-d\rho_{yaw}}{J_z}+\frac{\rho_s u}{m_T\left(u^2+v^2\right)}
\end{aligned} \tag{62}$$

More detailed mathematical steps to reach the solutions are given in the Appendix B. Finally, an individual braking torque could be isolated if all other braking torque is zero as illustrated below:

$$\begin{aligned}
\tau_{b3}&=\kappa_{Fxt3}^{-1}r_3\left(\chi_1-\chi_2+\chi_3\right)\ \text{if}\ \left\{\tau_{b1},\tau_{b2},\tau_{b4}\right\}=0\\
\tau_{b4}&=\kappa_{Fxt4}^{-1}r_4\left(\chi_1-\chi_2+\chi_3\right)\ \text{if}\ \left\{\tau_{b1},\tau_{b2},\tau_{b3}\right\}=0
\end{aligned} \tag{63}$$

By considering only rear wheels for breaking, the breaking controller algorithm for the vehicle stability control is given as follows

$$
\begin{aligned}
& \textit{Begin} \\
& \tau_{b1} = \tau_{b2} = 0 \\
& \tau_{b3} = \kappa_{Fxw3}^{-1} r_3 \left(\chi_1 - \chi_2 + \chi_3 \right) \\
& \textit{if} \quad \tau_{b3} > 0 \\
& \tau_{b3} = 0; \quad \tau_{b4} = \kappa_{Fxw4}^{-1} r_4 \left(\chi_1 - \chi_2 + \chi_3 \right) \\
& \textit{else} \\
& \tau_{b4} = 0 \\
& \textit{end}
\end{aligned}
\tag{64}
$$

3.1.2. ESC with Constant Longitudinal Speed Assumption

The ESC described above takes into account varying vehicle speed and the desired yaw acceleration and the wheel's rotational acceleration. However, since these are not explicitly available real time due to coupling effect. In order to overcome this problem, the controller takes the values from one frame ago. Therefore, there is a slight delay equal to the size of the frame rate (5ms) in the three values used. To build an ESC that does not depend on the three variables, it is possible to build a much simpler ESC that assumes constant vehicle speed. Though less practical than the former, the design of this controller cancels many terms out on the assumptions of a small sideslip angle, small steering angle, and a constant longitudinal velocity.

With aforementioned assumptions, the equations for sideslip angle of the vehicle and its derivative can be simplified as the following:

$$\beta = \frac{v}{u} \tag{65}$$

$$\dot{\beta} = \frac{\dot{v}}{u} \tag{66}$$

Then κ_{Fxti} and κ_{Fyti} of equation (62) are simplified to be:

$$\begin{aligned}
\kappa_{Fxt1} &= \frac{\rho_{yaw}}{J_z}\left(a\cos\delta_1 + c\sin\delta_1\right) + \sin\delta_1 \frac{\rho_s}{m_T u} \\
\kappa_{Fxt2} &= \frac{\rho_{yaw}}{J_z}\left(c\sin\delta_2 - b\cos\delta_2\right) + \sin\delta_2 \frac{\rho_s}{m_T u} \\
\kappa_{Fxt3} &= \frac{-b\rho_{yaw}}{J_z} \\
\kappa_{Fxt4} &= \frac{a\rho_{yaw}}{J_z} \\
\kappa_{Fyt1} &= \frac{\rho_{yaw}}{J_z}\left(c\cos\delta - a\sin\delta_1\right) + \cos\delta_1 \frac{\rho_s}{m_T u} \\
\kappa_{Fyt2} &= \frac{\rho_{yaw}}{J_z}\left(c\cos\delta_2 + b\sin\delta_2\right) + \cos\delta_2 \frac{\rho_s}{m_T u} \\
\kappa_{Fyt3} &= \frac{-d\rho_{yaw}}{J_z} + \frac{\rho_s}{m_T u} \\
\kappa_{Fyt4} &= \frac{-d\rho_{yaw}}{J_z} + \frac{\rho_s}{m_T u}
\end{aligned} \tag{67}$$

where u is no longer a function of time but a constant.

When the steering angle is small, the magnitude of the vehicle's longitudinal velocity does not change much and the lateral velocity is nearly zero. It is easy to see that the two ESC controllers shown above would produce very similar control torque if the value of u does not change and the value of v is near zero. However, as soon as the steering angle of the simulation goes over a certain threshold, the control force generated by the latter ESC becomes less reliable because the longitudinal velocity of the vehicle decreases significantly while the lateral velocity and sideslip rapidly increase.

3.1.3. ESC with Torque Vectoring or All Wheel Drive

For a conventional differential vehicle, the control torque can be applied in only one of the rear wheels. In other words, the control torque of one side should be zero while the other is non-zero in order to gain maximum yaw moment possible, because the wheels can only accelerate in one direction. However, the constraint disappears if the vehicle can control each wheel freely so that each wheel is free to accelerate in any direction simultaneously. For instances, a vehicle with torque vectoring option can freely transfer a torque from one wheel to the opposite wheel, and an electric vehicle with two separate motors in the rear axle can freely control each wheel's torque separately. With an assumption that such an option is available, the brake control torque calculated in Equation (63) can be split into two torques of opposite direction—an accelerating torque and a brake torque—before they are applied to the rear wheels. The new ESC can successfully provide the equally-effective yaw moment while significantly mitigating overall speed reduction of the vehicle compared to the conventional ESC. This concept has not been fully explored by this thesis, but a simple model that splits the calculated brake torque with a ratio of one half has been tested. As expected, compared to the conventional ESC, the new ESC showed much less vehicle speed reduction. The results are presented in the simulation section. In the future, more study on calculating the exact desired ratio between the accelerating torque and the brake torque is necessary. The proof of concept is available in the Simulation and Analysis section.

3.2. ATTITUDE MOTION CONTROL

The main goal of a vehicle attitude motion control system is to reduce the effect of centrifugal force in a cornering maneuver by tilting the opposite direction of the force. Tilting toward the center of the curve shifts the center of gravity, generating force by gravity that cancels out the centrifugal force to a certain degree. Reducing the effect of centrifugal force improves ride comfort in the lateral direction.

Not only does the AMC enhance the ride comfort, it also enhances vehicle safety by providing better road holding capability to the tires. In an uncontrolled passive vehicle's cornering maneuver, the vertical forces exerted on the outer wheels is greater than on the inner wheels because the lateral forces exerted on the car body tend to make the car tilt outward, which then causes the tire deflection of the outer wheels increase. The AMC, by setting the desired roll angle in the opposite of the passive angle, evens out the differences between the left and right tire deflections.

This objective is achieved using an optimal linear attitude controller with tracking control as explained in [2]. 7-DOF simple linear full car model which ignores the longitudinal, lateral and yaw motions of car body and rotational motion of wheel can be expressed by the continuous time state space vector equation as

$$\dot{\mathbf{x}} = \mathbf{Ax} + \mathbf{Bu} + \mathbf{Dw} \tag{68}$$

The definition of matrices A, B, and D are given in the Appendix C, and the discrete time state space vector equation is:

$$\mathbf{x}(k+1) = \mathbf{A_1x}(k) + \mathbf{B_1u}(k) + \mathbf{D_1w}(k) \tag{69}$$

where A_1 = I+ Adt, B_1 = Bdt, and D_1 = Ddt. With the state space, **x**, defined in (13) of the previous section, the desired state vector $\mathbf{x_d}$ is given as the following:

$$\mathbf{x_d} = [0, \theta_d, \phi_d, 0,0,0,0,0,0,0,0,0,0,0,0,0,0]^T \tag{70}$$

where x_{d2} and x_{d3} are the desired pitch and roll angles respectively. The disturbance input vector, **w**, is defined as:

$$\mathbf{w} = [\dot{z}_{o1}, \dot{z}_{o2}, \dot{z}_{o3}, \dot{z}_{o4}, M_x, M_y]^T \tag{71}$$

where $w_{1\sim4}$ are the vertical velocities of the tire-ground contact points caused by road disturbances, and $w_{5\sim6}$ are summations of longitudinal and that of lateral body forces applied to the suspension mounting points of the vehicle. It is assumed that all of the disturbances are known before the calculation of the control forces.

With the predetermined disturbances, the desired pitch and roll angles in (70) can be calculated by considering the effect of the mass times gravity, and the method is explained thoroughly at the end of this section.

The active tracking optimal controller minimizes the performance index *J*, which is composed of acceleration, roll acceleration, pitch acceleration, suspension rattle spaces, errors between desired and actual angle of car body, road holding forces, and control forces as given below.

$$J = \lim_{T\to\infty}\frac{1}{2T}\int_0^T [\rho_1\dot{x}_1^2 + \rho_2\dot{x}_4^{\ 2} + \rho_3\dot{x}_5^{\ 2} + \rho_4 x_6^{\ 2} + \rho_5 x_7^{\ 2} + \rho_6 x_8^{\ 2} + \rho_7 x_9^{\ 2} + \rho_8\left(x_{d2} - x_2\right)^2$$
$$+\rho_9\left(x_{d3} - x_3\right)^2 + \rho_{10}x_{10}^2 + \rho_{11}x_{11}^2 + \rho_{12}x_{12}^2 + \rho_{13}x_{13}^2 + \rho_{14}u_1^2 + \rho_{15}u_2^2 + \rho_{16}u_3^2 + \rho_{17}u_4^2]\mathrm{dt} \tag{72}$$

By expanding and rearranging the performance index given above, the optimal control matrices Q, R, N1, N2, M1, and M2, which are used in the following discrete-time quadratic control equation, can be determined.

$$\begin{aligned} J = &\frac{1}{2}\left(\mathbf{x_d}(n) - \mathbf{x}(n)\right)^{\mathbf{T}}\mathbf{S}\left(\mathbf{x_d}(n) - \mathbf{x}(n)\right) \\ &+\sum_{\mathbf{k=0}}^{\mathbf{n-1}}\frac{\mathbf{1}}{\mathbf{2}}\Big\{\left(\mathbf{x_d}(k) - \mathbf{x}(k)\right)^{\mathbf{T}}\mathbf{Q}\left(\mathbf{x_d}(k) - \mathbf{x}(k)\right) + \mathbf{u}^{\mathbf{T}}(k)\mathbf{Ru}(k) + \mathbf{w}(k)^{\mathbf{T}}\mathbf{M_2w}(k) \\ &+\mathbf{2}\left(\mathbf{x_d}(k) - \mathbf{x}(k)\right)^{\mathbf{T}}\mathbf{N_1u}(k) + \mathbf{2}\left(\mathbf{x_d}(k) - \mathbf{x}(k)\right)^{\mathbf{T}}\mathbf{N_2w}(k) + \mathbf{2w}(k)^{\mathbf{T}}\mathbf{M_1u}(k)\Big\} \end{aligned} \tag{73}$$

The elements of each matrix are given in Appendix C. Minimizing Equation (72) results in the following optimal control force:

$$\mathbf{u}(k) = -\left(\mathbf{R} + \mathbf{B_1}^{\mathbf{T}}\mathbf{PB_1}\right)^{-1}\left\{\left(\mathbf{B_1}^{\mathbf{T}}\mathbf{PA_1} - \mathbf{N_1}^{\mathbf{T}}\right)\mathbf{x}(k) + \left(\mathbf{M_1}^{\mathbf{T}} + \mathbf{B_1}^{\mathbf{T}}\mathbf{PD_1}\right)\mathbf{w}(k) + \mathbf{N_1^T x_d}(k) + \mathbf{B^T b_R}^{\mathbf{T}}(k+1)\right\} \tag{74}$$

where $\mathbf{P}$ is derived by solving the Algebraic Riccati equation:

$$\mathbf{P} = \mathbf{A}^{\mathbf{T}}\mathbf{PA} - (\mathbf{A}^{\mathbf{T}}\mathbf{PB})(\mathbf{R} + \mathbf{B}^{\mathbf{T}}\mathbf{PB})^{-1}(\mathbf{B}^{\mathbf{T}}\mathbf{PA}) + \mathbf{Q} \tag{75}$$

and $\mathbf{b_R}$ is derived by solving the feed-forward excitation function, which includes future information of the system states, desired states, and disturbance states.

After substituting $\mathbf{u}$ into Equation (69), the closed loop system equation of the simplified linear full car model is obtained as:

$$\begin{aligned}
\mathbf{x}(k+1) &= (\mathbf{A_1} + \mathbf{B_1K_1})\mathbf{x}(k) + \mathbf{B_1K_2x_d}(k) + (\mathbf{D_1} + \mathbf{B_1K_3})\mathbf{w}(k) + \mathbf{B_1K_4b_R}^{\mathbf{T}}(k+1) \\
\mathbf{K_1} &= -\left(\mathbf{R} + \mathbf{B_1}^{\mathbf{T}}\mathbf{PB_1}\right)^{-1}\left(\mathbf{B_1}^{\mathbf{T}}\mathbf{PA_1} - \mathbf{N_1}^{\mathbf{T}}\right) \\
\mathbf{K_2} &= -\left(\mathbf{R} + \mathbf{B_1}^{\mathbf{T}}\mathbf{PB_1}\right)^{-1}\mathbf{N_1^T} \\
\mathbf{K_3} &= -\left(\mathbf{R} + \mathbf{B_1}^{\mathbf{T}}\mathbf{PB_1}\right)^{-1}\left(\mathbf{M_1}^{\mathbf{T}} + \mathbf{B_1}^{\mathbf{T}}\mathbf{PD_1}\right) \\
\mathbf{K_4} &= -\left(\mathbf{R} + \mathbf{B_1}^{\mathbf{T}}\mathbf{PB_1}\right)^{-1}\mathbf{B_1}^{\mathbf{T}}
\end{aligned} \tag{76}$$

where $K_{1\text{-}4}$ are control gains for the $\mathbf{x}$, $\mathbf{x_d}$, $\mathbf{w}$, and $\mathbf{b_R}$, respectively.

3.2.1. Desired Roll and Pitch Angles

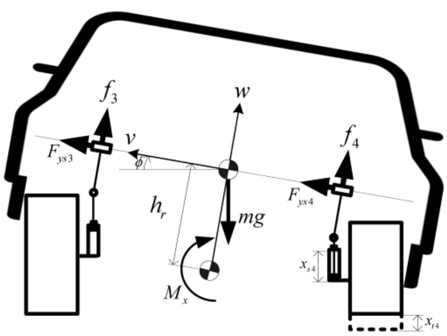

Figure 7: The rear view of the 7-DOF linear model

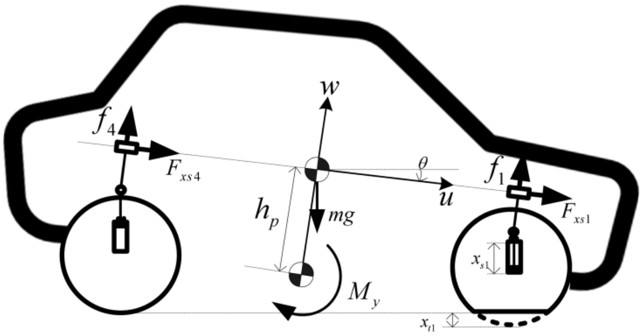

Figure 8: The side view of the 7-DOF linear model

The desired roll angle and pitch angle are assumed to be predetermined. They are calculated by taking into account the longitudinal and lateral forces exerted on the tire-ground contact points. As illustrated in **Figure 7** and **Figure 8**, the pitching and rolling momentum exerted on the car body are defined to be the product of the ground forces and the rolling and pitching centers as the following:

$$\begin{aligned} M_x &= -h_r \sum_{i=1}^{4} F_{ysi} \\ M_y &= h_p \sum_{i=1}^{4} F_{xsi} \end{aligned} \tag{77}$$

where h_r and h_p are the height of the roll and pitch centers respectively. In order to cancel out the momentums, the desired pitching and rolling momentums would be the exactly the opposite as shown below:

$$\begin{aligned} M_{xd} &= -M_x \\ M_{yd} &= -M_y \end{aligned} \tag{78}$$

The objective of the AMC is to generate M_{xd} and M_{yd} using the gravitational force mg. The momentum is the product of mg and the radius perpendicular to the direction of *mg* as shown below:

$$M_{xd} = mgh_r \sin\phi_d$$
$$M_{yd} = mgh_p \sin\theta_d \tag{79}$$

Substituting M_x and M_y and solving for desired roll and pitch angles would result in the following:

$$\phi_d = \sin^{-1}\left(\frac{-M_x}{mgh_r}\right)$$
$$\theta_d = \sin^{-1}\left(\frac{-M_y}{mgh_p}\right) \tag{80}$$

It is to note that the desired roll and pitch angles generated by this equation may be above the realistic threshold. It is assumed that the vehicle has the roll and pitch limits to be 20 degrees and 10 degrees, respectively. This definition of limits puts an upper boundary on AMC's capability to cancel out centrifugal forces and to evenly distribute the vertical tire forces. If this roll and pitch angle limits are removed, the controller may work more effectively, allowing the vehicle to behave much like a motor cycle.

3.2.2. Notes on Preview Information

According to [2], 0.3 seconds of preview information provides significantly more reliable control forces in terms of tracking control. The study presents three types of preview information which are considered for this study's simulations: 1) deterministic information, 2) rate of change information, and 3) limited information. The deterministic information assumes that the information in interest (F_{xgi} and F_{ygi} in this case) is entirely known prior to simulations. This method naturally provides the best results in simulations. However, in the real world, it is not realistic to have the exact future information available at all times. Therefore, the practicality of the deterministic information may be put to debate.

The rate of change information assumes that the rate of change of data at each time frame will persist for the preview interval. If the vehicle is currently accelerating, the preview information assumes that the vehicle will continue to accelerate at a same rate for the preview interval. This information is incomplete compared to the deterministic information, but is the most realistic and practical method to apply in real world. This information shows best performances in situations with slow rate of change such as soft S-turn maneuvers. For the systems that have states that has high frequency of abrupt changes such as drones, the reliance on rate of change information alone is not advisable.

The limited information assumes that the system's current state will be nearly constant for the preview interval. It is the simplest form of use of preview information and shows the least favorable performance. This information shows the best performance in steady state environments with minimal rate of change such as in steady curve maneuvers.

Though it would be possible to apply each of the three types of information to the design of AMC and compare the results, the study could be done some other time in the future. Because the focus of this study is on the effects of integration of AMC and ESC on a nonlinear full vehicle model, this study assumes that the deterministic information is available for all simulations.

3.3. INTEGRATION OF THE TWO CONTROLLERS

As have been previously mentioned, the ESC and AMC developed using the 7-DOF models are applied to 14-DOF nonlinear model in order to be evaluated on the effects of integration. Since ESC does not depend on vertical motions of the vehicle, the static differences in tire and suspension deflections does not affect the performance of ESC. Therefore, the ESC designed for 7-DOF model can be directly applied to the 14-DOF model without any modification. However, the AMC, which depends heavily on vertical motions of the vehicle, requires a modification before being applied to the 14-DOF model.

3.3.1. Differential Equation for 14-DOF Model

The nonlinear differential equation is expressed as the following:

$$\mathbf{E}\dot{\mathbf{x}}_{\mathbf{n}} = \mathbf{F}\left(\mathbf{x}_{\mathbf{n}}\right) \tag{81}$$

where the 25 states of the nonlinear differential system, $\mathbf{x}_n$, is given in (25), and the disturbance vector is given as the following:

$$\mathbf{w}_{\mathbf{n}} = \left[w_{g1}, w_{g2}, w_{g3}, w_{g4}, \delta, \tau\right] \tag{82}$$

where $w_{g1\sim4}$ are vertical road disturbance, δ the steering angle input, and τ

the braking torque input.

Using 4th order Runge-Kutta algorithm, the nonlinear differential equation can be solved as the following:

$$\mathbf{x_n}(k+1) = \mathbf{x_n}(k) + \frac{\Delta t}{6}\left(\mathbf{k_1} + 2\mathbf{k_2} + 2\mathbf{k_3} + \mathbf{k_4}\right) \tag{83}$$

$$\begin{aligned}
\mathbf{k_1} &= \mathbf{Ex}^{-1}\mathbf{F}\left(\mathbf{x_n}(k)\right) \\
\mathbf{k_2} &= \mathbf{Ex}^{-1}\mathbf{F}\left(\mathbf{x_n}(k) + \frac{\Delta t}{2}\mathbf{k_1}\right) \\
\mathbf{k_3} &= \mathbf{Ex}^{-1}\mathbf{F}\left(\mathbf{x_n}(k) + \frac{\Delta t}{2}\mathbf{k_2}\right) \\
\mathbf{k_4} &= \mathbf{Ex}^{-1}\mathbf{F}\left(\mathbf{x_n}(k) + \Delta t\mathbf{k_3}\right)
\end{aligned} \tag{84}$$

The $\mathbf{k}_{1\text{-}4}$ are strictly for the Runge-Kutta algorithm and are unrelated to the control gains in Equation (76).

3.3.2. Consideration of Static Deflections

One of the critical differences between the 7-DOF linear model for AMC and the 14-DOF nonlinear model is that the former does not consider static deflections of tires and suspensions. The 7-DOF linear model assumes the equilibrium state of the vehicle, and the initial values for suspension and tire deflections are all zeros.

In comparison, the nonlinear model has the static deflections because its equilibrium state takes into account the effects of *mg*. The nonlinear model's initial conditions for the tire and suspension deflections, therefore, must be calculated as shown below:

$$
\begin{aligned}
x_{t1,static} &= \frac{mgd}{2k_1\left(c+d\right)} \\
x_{t2,static} &= \frac{mgd}{2k_2\left(c+d\right)} \\
x_{t3,static} &= \frac{mgc}{2k_3\left(c+d\right)} \\
x_{t4,static} &= \frac{mgc}{2k_4\left(c+d\right)}
\end{aligned}
\tag{85}
$$

$$
\begin{aligned}
x_{s1,static} &= \left(\frac{md}{2\left(c+d\right)}+m_{u1}\right)\frac{g}{k_{t1}} \\
x_{s2,static} &= \left(\frac{md}{2\left(c+d\right)}+m_{u2}\right)\frac{g}{k_{t2}} \\
x_{s3,static} &= \left(\frac{mc}{2\left(c+d\right)}+m_{u3}\right)\frac{g}{k_{t3}} \\
x_{s4,static} &= \left(\frac{mc}{2\left(c+d\right)}+m_{u4}\right)\frac{g}{k_{t4}}
\end{aligned}
\tag{86}
$$

where $x_{n14\sim17}$ are the suspension deflections and $x_{n18\sim21}$ the tire deflections. When running the nonlinear model with the AMC controller disabled, the simulation runs smoothly. However, the problem arises when AMC is enabled in the 14-DOF nonlinear model. The AMC designed in the linear model has functionality to output control forces to evenly distribute the vertical tire forces. When applied to the 14-DOF nonlinear model, the controller detects the static deflections and attempts to make the deflections zero, causing not only the massive spikes in the beginning, but also a static error throughout the simulations. In order to fix this issue, a copy of $\mathbf{x}_n$ is newly defined as $\mathbf{x}_{\mathbf{ntmp}}$, so that prior to whenever the control force $\mathbf{u}$ is calculated in the following manner,

$$\mathbf{u}(k) = \mathbf{K_1 x_{ntmp}}(k) + \mathbf{K_2 x_d}(k) + \mathbf{K_3 w}(k) + \mathbf{K_4 b_R}^{\mathbf{T}}(k+1) \tag{87}$$

At each iteration before being applied in the calculation of $\mathbf{u}$, the $\mathbf{x}_{\mathbf{ntmp}}$ is modified as the following:

$$\begin{aligned}
x_{n14tmp}(k) &= x_{n14}(k) - \frac{mgd}{2k_1(c+d)} \\
x_{n15tmp}(k) &= x_{n15}(k) - \frac{mgd}{2k_2(c+d)} \\
x_{n16tmp}(k) &= x_{n16}(k) - \frac{mgc}{2k_3(c+d)} \\
x_{n17tmp}(k) &= x_{n17}(k) - \frac{mgc}{2k_4(c+d)}
\end{aligned} \tag{88}$$

$$\begin{aligned}
x_{n18tmp}(k) &= x_{n18}(k) - \left(\frac{md}{2(c+d)} + m_{u1}\right)\frac{g}{k_{t1}} \\
x_{n19tmp}(k) &= x_{n19}(k) - \left(\frac{md}{2(c+d)} + m_{u2}\right)\frac{g}{k_{t2}} \\
x_{n20tmp}(k) &= x_{n20}(k) - \left(\frac{mc}{2(c+d)} + m_{u3}\right)\frac{g}{k_{t3}} \\
x_{n21tmp}(k) &= x_{n21}(k) - \left(\frac{mc}{2(c+d)} + m_{u4}\right)\frac{g}{k_{t4}}
\end{aligned} \tag{89}$$

This method allows AMC to ignore the tire and suspension static deflections of the 14-DOF nonlinear model.

4. SIMULATION AND ANALYSIS

In this section, various comparisons are made between wide ranges of simulations with different conditions in order to evaluate the effectiveness of the controllers on the vehicle safety, lateral stability, handling capability, and ride comfort. The 14-DOF vehicle model without any control input is denoted as 'PAS,' the model with only electronic stability control input applied as 'ESC,' the model with only attitude motion control input applied as 'AMC,' and the model with both ESC and AMC applied as 'ESC+ AMC.'

Three types of steering conditions are defined for 14-DOF nonlinear full vehicle model: over-steering, under-steering, and neutral-steering. The constants and conditions used in the simulation are listed in **Table 4.1** available below:

Table 4.1: Vehicle Parameters

Variable	Name	Steering Type		
		Over-steering	Under-steering	Neutral-steering
m	Sprung mass	1440kg	1440kg	1440kg
m_{ui}	Wheel mass	80kg	80kg	80kg
J_x	Sprung mass roll inertia	900kg m^2	900kg m^2	900kg m^2
J_y	Sprung mass pitch inertia	2000kg m^2	2000kg m^2	2000kg m^2
J_z	Sprung mass yaw inertia	2000kg m^2	2000kg m^2	2000kg m^2
k_{ti}	Tire stiffness	200kN m^{-1}	200kN m^{-1}	200kN m^{-1}
r_o	Maximum tire radius	0.285m	0.285m	0.285m
h	Sprung mass c.g. height	0.75m	0.75m	0.75m
h_r	c.g. distance to roll center	0.6m	0.6m	0.6m
h_p	c.g. distance to pitch center	0.7m	0.7m	0.7m
C_{ai}	Tire cornering stiffness	26k N m^{-1}	26k N m^{-1}	26k N m^{-1}
C_{ti}	Tire longitudinal stiffness	100k N m^{-1}	100k N m^{-1}	100k N m^{-1}
a	c.g. distance to right axle	0.75m	0.75m	0.75m
b	c.g. distance to left axle	0.75m	0.75m	0.75m
c	c.g. distance to front axle	1.016m	1.524 m	1.25 m
d	c.g. distance to rear axle	1.524m	1.016 m	1.25 m
k_1, k_2	Front suspension stiffness	35kN m^{-1}	30k N m^{-1}	3.25k N m^{-1}
k_3, k_4	Rear suspension stiffness	30kN m^{-1}	35k N m^{-1}	3.25k N m^{-1}
b_1, b_2	Front susp. damping coefficient	2.5kNs m^{-1}	2k Ns m^{-1}	2.25k Ns m^{-1}
b_3, b_4	Rear susp. damping coefficient	2k Ns m^{-1}	2.5k Ns m^{-1}	2.25k Ns m^{-1}

4.1. TIRE MODEL COMPARISON

Two types of tire models are compared in this thesis: the linear tire model and pacejka tire model. The linear tire model simply outputs a product of slip variable (sideslip angle or longitudinal slip ratio), tire stiffness coefficient (cornering or longitudinal stiffness), and vertical force distribution ratio. On the other hand, the pacejka model has its foundation on arbitrary equations based on experimental data. The linear tire model is simple and useful, but it comes with limitations. **Figure 9** and **Figure 10** illustrate the comparison between the longitudinal and lateral tire forces generated by the linear tire model and the pacejka tire model. Both models show upper (F_{zg} = 8,000 N) and lower (F_{zg} = 2,000 N) boundaries.

Figure 9: Longitudinal force generated by the two tire models. Bigger value of vertical force (Fzg) creates steeper forces. Negative and positive longitudinal slip ratios mean decelerating and accelerating respectively.

Figure 10: Lateral force generated by the two tire models. Bigger value of vertical force (Fzg) creates steeper forces. Negative and positive sideslip angles mean slipping to left and right side of the tire respectively.

When the magnitudes of steering angle and vehicle speed are reasonably low, so that the small sideslip angle and longitudinal slip ratio may be assumed, the linear tire model shows acceptable behavior, generating similar results as the pacejka model. However, as shown in **Figure 9** and **Figure 10**, the longitudinal and lateral tire forces, F_{xti} and F_{yti}, of linear tire model increase at a much faster rate in high sideslip and longitudinal slip regions. The effect of this rapid rate of increase is demonstrated in the **Figure 11** through **Figure 18**. It is experimentally proven on the 14-DOF nonlinear full vehicle model that the pacejka tire model is much more reliable than the linear tire model. As shown in Figures (4.3) to (4.5), given small steering angle (0.3°) and slow speed (20km/h), the type of tire models has negligible effect on the longitudinal and lateral forces generated. However, given significantly bigger angle (4°) and faster speed (80km/h) as in Figures (4.6) to (4.8), the linear tire model does not generate reasonable force outputs while the pacejka tire model still does. Because of its better reliability, only the pacejka tire model is used for the simulations in the following sections.

Figure 11: Steering input for 14-DOF nonlinear full vehicle model with neutral steering condition.

Figure 12: Front left longitudinal tire forces generated by the two models. All four wheels have similar profiles.

Figure 13: Front left lateral tire forces generated by the two models. All four wheels have similar profiles.

Figure 14: Steering input for 14-DOF nonlinear full vehicle model with neutral steering condition.

Figure 15: Front left longitudinal tire forces generated by the two models.

Figure 16: Front left lateral tire forces generated by the two models.

4.2. THE EFFECTS OF ESC

Three different types of ESC are introduced in this thesis. The first is a conventional ESC for vehicles with differentials. This model is the simplest model which makes many assumptions such as constant longitudinal vehicle velocity and constant rotational velocity of each wheel. A more complex ESC is developed in order to take into account the changing vehicle velocity and acceleration of each wheel, but the performance difference was negligible, thus the conventional ESC is used for simplicity. More research is necessary in order to explore the full potential of the ESC's capability to utilize variable speed.

The two aforementioned ESCs both have a major disadvantage of inevitable speed reduction. This is because the only available source of control forces is the braking force. In attempt to solve this major drawback of the original ESC, a new ESC is proposed with an assumption that each wheel is motor-driven as in common electric vehicles available today. The new concept is simply that the braking control torque calculated by the original ESC can be split in half and provided to the opposite wheel as the accelerating control torque. Doing so not only generates the same yawing momentum required by the controller, but it also minimizes the speed reduction present in original ESC.

To evaluate the performance of this ESC, an S-Turn maneuver is simulated on the 14-DOF nonlinear full vehicle model with the initial speed of 50km/h and the steering angle input given as in **Figure 17**. In order to maximize the clarity of the ESC performance, an over-steering condition is applied to the vehicle model.

As shown in **Figure 18**, the old ESC's longitudinal vehicle velocity drops to almost half of its initial velocity only 5 seconds into the simulation. This is not just a simple undesired effect, but it can potentially be a significant issue because the ESC assumes constant vehicle velocity in its control torque calculations. The new ESC significantly minimizes velocity reduction compared to the old ESC. **Figure 19** shows that both ESCs have outstanding performance in following the reference yaw rate, and the advantage of the new ESC is not so apparent. In **Figure 20**, however, it is apparent that the new ESC follows the reference yaw angle more closely than the old ESC does.

Figure 17: Steering input of the S-turn simulation at 50km/h

Figure 18: Change of vehicle longitudinal velocity over time for each simulation

Figure 19: Reference and measured yaw rate of each simulation

Figure 20: Reference and measured yaw angle of each simulation

Following the reference yaw rate closely comes with a cost. An ESC designer often needs to compromise between the yaw rate and sideslip angle of the vehicle by assigning proper weighting factors that decide which to prioritize. If yaw rate is the priority, the vehicle will need a strong instantaneous yawing momentum, which inevitably results in bigger sideslip angle. On the other hand, if zero sideslip angle is the priority, the vehicle should not make rapid turns, which results in slower response time for yaw rates. In this thesis, bigger emphasis is put on following the reference yaw rate instead of following the zero sideslip angle. Therefore, both ESC shows satisfying results in terms of following the yaw rate, but the sideslip reduction is limited. **Figure 21** and **Figure 22** show the front and rear tire sideslip angles. It is shown that the new ESC is less effective in reducing the sideslip angle compared to the old. This is because the old ESC can reduce the sideslip angle and still follow the reference yaw rate at the cost of the longitudinal velocity. The new ESC does not allow the longitudinal velocity to reduce significantly. Although the new ESC shows bigger sideslip angles than the old ESC, it follows the reference yaw rate without decrease in the vehicle speed while keeping the sideslip angle the same level or even smaller than the uncontrolled vehicle, which further proves the new ESC's effectiveness.

Figure 21: Sideslip angle of the rear right wheel

Figure 22: Sideslip angle of the front right wheel

As previously stated, the new ESC is still in its developmental stage and currently remains as only a concept. **Figure 23** and **Figure 24** show the control torque output of the original and new ESCs. The new ESC splits the control torque calculated in the original algorithm in half and provides it to the other wheel as an acceleration torque. For example, at Time = 1 second of the figures, the rear left control torque is calculated to be -1000Nm in the original ESC, and the new ESC splits the torque in half and provide 500Nm torque to the opposite wheel as an acceleration torque.

Figure 23: Control torque of the rear left wheel

Figure 24: Control torque of the rear right wheel

Finally, the front tire deflections are featured in **Figure 25**because the effect of the controllers on tire deflections is one of important topics in this thesis. As shown in the figure, there is no apparent effect the controller exerts on the tire deflections.

Figure 25: Tire deflections are not very much affected by ESC alone.

4.3. THE EFFECT OF AMC

The main purpose of attitude motion controller is to generate moment using the vehicle's attitude and gravity in order to cancel out the moment created by centrifugal force and longitudinal force. This concept is very similar to that of an ice skater tilting his or her body in the opposite direction of the centrifugal force in order to create a moment using the body mass, the tilt angle, and the gravity. One of the limitations of AMC, however, is that it shows rather slow response time. For example, if the AMC is tested in the

S-turn simulations as in the previous section, it will generate unsatisfactory results. In order to evaluate its effectiveness, the AMC is simulated on a 14-DOF nonlinear full vehicle model with neutral steering condition at 80km/h. The steady curve steering angle of 2 degrees is given as input as in **Figure 26**.

Figure 26: Steering input for 14-DOF nonlinear full vehicle model with neutral steering condition.

Figure 27 and **Figure 28** illustrate the desired roll and pitch angles. Unlike the ice skater or a motor cycle, ground vehicles have much more limited range of roll and pitch angles due to its body dimensions. For this simulation, as shown in **Figure 27**, in order to generate enough moment to entirely cancel out the rolling moment created by the centrifugal force, the vehicle needs to be able to tilt to -50 degrees. This is highly unrealistic because the vehicle has limited length of each suspension and radius of the each tire. It has been found from trial and error that the stable roll angle threshold for this specific 14-DOF nonlinear model is 25 degrees. If the vehicle crosses this threshold, it will create in illogical results such as negative suspension or tire deflections and cause the simulation to crash. The same idea applies to the pitch angle of the vehicle, setting its threshold to be 10 degrees. However, like how it is much more likely to have a vehicle to roll over than pitch over, it is rare for the desired pitch angle to exceed the given threshold.

Figure 27: In order to generate enough moment to cancel all moment created by the centrifugal force, the vehicle needs to tilt to -50 degrees

Figure 28: The reference pitch angle has the threshold of 10 degrees.

Also shown in the figures are actual roll and pitch angles of the passive vehicle model and the vehicle model with AMC applied. Notice that the magnitudes of the actual roll and pitch angles fall short of the required roll and pitch angles. This is because the controller has to consider not only the desired roll and pitch angles but also other factors such as tire and suspension deflections and limit of control forces. The order of priority is determined by the weighting factors in the performance index of Equation (72). The weighting factors are arbitrarily decided by the designer.

Figure 29: Total roll moment of controlled and uncontrolled vehicle models

Figure 30: Total pitch moment of controlled and uncontrolled vehicle models

Figure 31: Left and right front tire deflections of controlled and uncontrolled vehicle models

Figure 32: left and right front vertical tire forces of controlled and uncontrolled vehicle models

Figure 29 through **Figure 36** all illustrate the effects caused by the AMC applied. **Figure 29** and **Figure 30** show the total roll and pitch moments created by the passive vehicle and the AMC-applied vehicle. As stated previously, the total moments cannot be completely cancelled out because of the upper boundary of the roll and pitch angles due to the vehicle model's dimensional limits. The vertical tire forces heavily depend on the tire deflection of the vehicle. As shown in **Figure 31**, the difference between left and right tire deflections of the passive model is significantly big. This means that, at peak point where Time = 3 seconds, the right tire will receive over 7,000 N of vertical force while the left tire will receive barely 1,500 N, according to **Figure 32**. On the other hand, the difference between the left and right vertical tire forces of the AMC-applied vehicle at the same time frame is only 2,100 N, a significant drop compared to the passive model's 5,700 N. As was illustrated in **Figure 9** and **Figure 10**, regardless of the tire model, the magnitude of the vertical tire force is very influential to the longitudinal and lateral tire force outputs. This leads to a hypothesis that states, although the attitude motion controller only controls vertical motions of the vehicle, it does have indirect influence over the longitudinal and lateral motions of the vehicle.

The hypothesis can be strengthened by analyzing other states of the vehicle model relating to the vehicle's longitudinal and lateral motions. First, **Figure 33** shows a slight reduction in the vehicle's longitudinal deceleration caused by F_{xgi} and F_{ygi} during cornering. **Figure 34** shows a more significant reduction is lateral velocity of the vehicle. As shown in Equation (52), the sideslip angle of the vehicle has direct relationship with the lateral and longitudinal velocity. An increase in longitudinal velocity and decrease in lateral velocity means a definite decrease in sideslip angle of the vehicle. Furthermore, **Figure 35** shows that the lateral forces of the left and right front tire are much more balanced in AMC model in comparison to that of passive model. The difference between the left and right tire forces of AMC vehicle is less than 1,000 N, while that of passive vehicle is 3,200 N. These figures directly prove the cause and effect relationship between vertical tire forces and lateral tire forces. More balanced tire forces means better road holding capability. This is again demonstrated by **Figure 36**, which shows much reduced sideslip angle of the tire. Each of the four tires of the simulation shows very similar behavior.

Figure 33: Effects of AMC on longitudinal velocity

Figure 34: Effects on lateral velocity

Figure 35: Left and right front lateral tire forces

Figure 36: Front left tire sideslip. Each tire has a similar profile.

4.4. THE EFFECTS OF INTEGRATIONS OF ESC AND AMC

In the previous sections, the independent effectiveness of the electronic stability controller and attitude motion controller is demonstrated. ESC is designed in a 7-DOF model that only takes into account parallel-to-the-ground motions. ESC does not produce any beneficial effect on vehicle's vertical motion (i.e. rapid yaw rate only creates bigger roll angles), but it heavily depends on the tire forces because the only way for the ESC to control the vehicle is through the tire-ground frictions forces of rear two wheels. On the other hand, AMC is designed in a 7-DOF model that only takes into account vertical motions. Although AMC has direct effects on only the vertical forces using active suspensions, AMC may indirectly assist ESC by evenly distributing vertical tire forces, which are directly related to longitudinal and lateral tire force calculations. By evenly distributing the vertical tire forces, the vehicle's road holding capability increases along with more stability.

The effects of the integration of ESC and AMC are demonstrated by conducting simulations on a 14-DOF nonlinear full vehicle model with over-steering condition at 80km/h. The steering input is given as shown in **Figure 37**. The integrated controller, as shown in **Figure 38**, still produces satisfying results in evenly distributing tire forces, reducing the average difference between the left and right tire deflections to 0.05m compared to ESC model's 0.15m and passive model's 0.25m. The 0.1m reduction of tire deflection difference in the ESC model compared to the passive model is a result of speed reduction, which is not necessarily considered as improvement. Because the tire deflections have direct relationship with the vertical forces of the tires, the vertical tire forces of the integrated controller is much more evenly distributed compared to the other two models as shown in **Figure 39**. The evenly distributed forces are then used to generate lateral forces which are illustrated in **Figure 40**. In the passive model, the peak difference between the left and right lateral tire forces is around 1,700 N in passive model, 600N in ESC only model, and a mere 200 N in the integrated model. This well-distributed tire forces results in better road holding capability which then improves ESC's performance.

Figure 37: Steering input for 14-DOF nonlinear full vehicle model with over-steering condition.

Figure 38: Front left and right tire deflections

Figure 39: Front left and right vertical tire forces.

Figure 40: Rear left and right lateral tire forces.

Figure 41: Reference and measured yaw rate of each simulation

Figure 42: Vehicle sideslip angle comparison for each simulation.

The ESC is already optimized in following the yaw rate, thus there is not much apparent improvement shown in **Figure 41**. However, the effect of enhanced road holding capability is more clearly shown in **Figure 42**, where the sideslip angle of the vehicle is significantly reduced for the model equipped with the integrated controller compared to the others. The root mean square value of the sideslip of each simulation is calculated in order to help with more clear understanding of the sideslip reduction.

$$\begin{aligned}
\beta_{RMS,AMC+ESC} &= \sqrt{\frac{1}{N}\sum_{n=1}^{N}\left|\beta_{AMC+ESC,n}\right|^2} = 0.0995 \\
\beta_{RMS,ESC} &= \sqrt{\frac{1}{N}\sum_{n=1}^{N}\left|\beta_{ESC,n}\right|^2} = 0.2441 \\
\beta_{RMS,passive} &= \sqrt{\frac{1}{N}\sum_{n=1}^{N}\left|\beta_{passive,n}\right|^2} = 1.3701
\end{aligned} \tag{90}$$

where N is the number of sample size of each simulation.

4.5. STABILITY TESTS

In order to further prove the advantage of the integrated controller, stability test for each model is conducted as demonstrated in the face portraits of **Figure 43** through **Figure 46**. The stability tests help defining the simulation models' region of stability. Each point (x or o) is the initial point of an independent simulation with the initial conditions set with the longitudinal velocity at 50km/h and the corresponding yaw rate and lateral velocity. All other disturbances inputs such as steering wheel angle or external torque are set to zero. The goal of the simulation is to observe if the model can reach the equilibrium point (yaw rate = 0; lateral velocity = 0) within the time limit with given initial conditions. Several conditions are defined to identify unstable trials. If the magnitudes of vehicle velocity, yaw rate, roll angle, and pitch angle exceed predefined thresholds at any point of each trial, or if the vehicle model has not reached the equilibrium point at the end of each trial, the trial is deemed a failure and marked with x before the next trial begins. For example, in **Figure 43**, if the passive vehicle model begins trial with initial longitudinal velocity of 50km/h, yaw rate of 40 deg/s, and lateral velocity of -4m/s, the trial does not reach the equilibrium point and is marked with x, whereas the trial with initial yaw rate of 60deg/s and zero lateral velocity does reach the equilibrium point and is marked with o. Note, however, that *all* simulations can reach the equilibrium point given enough time because the tire friction forces continuously reduce the vehicle speed over time. The stability tests only check if the system is able to reach the equilibrium point *within a specific time limit*. Thus comparing the stability test plots shows the relative stability, not absolute stability.

It is important to note the difference in the area of region of stability (marked with o) in each model's simulation. The ESC in **Figure 44** slightly improves the vehicle model's tolerance to both the lateral velocity and the yaw rate, whereas the AMC in **Figure 45**, slightly improves the yaw rate tolerance, seem to worsen the lateral velocity tolerance compared to the passive model.

Also notable is the twitchy, rough lines present in the AMC and ESC+AMC model simulations. This is due to abrupt change in control forces directly influences the lateral tire forces. Although the crash threshold for the roll angle is set to 25 degrees, the controller is free to utilize all the available control force in attempt to make the vehicle stable, thus abrupt changes in tire forces are inevitable.

Finally, **Figure 46** shows the face portrait of the stability test results of the integrated controller with satisfying outcome. The integration of ESC and AMC dramatically increased the region of stability compared to any other figures. Although the rough lines may seem to imply that the vehicle is unstable, as long as the initial point of the line is marked with o, the vehicle stayed within all of the thresholds of yaw rate, velocity, roll angle, and pitch angle, and reached the equilibrium point within the time limit.

Figure 43: Face portrait of stability test for the passive model.

Figure 44: Face portrait of stability test for the ESC only model.

Figure 45: Face portrait of stability test for the AMC only model.

Figure 46: Face portrait of stability test for the integrated controller model.

5. CONCLUSION

In this paper, the main objective was to present an integration of ESC and AMC, and to analyze its synergistic effects on vehicle safety, lateral stability, handling capability, and ride comfort using a full vehicle nonlinear model. The AMC was designed using 7-DOF vertical model to improve the vehicle handling capability and lateral ride comfort by tilting against the direction of the rolling and pitching moment caused by centrifugal and longitudinal forces which in turn evenly distributes the vertical tire forces. This technique mitigates the lateral and longitudinal accelerations exerted on the passenger during cornering and braking maneuvers. As presented in the simulations, the AMC successfully evened out tire deflections and reduced acceleration on passenger during cornering, but was unable to provide vehicle safety and lateral stability due to large sideslip angle and yaw-rate due to limited roll and pitch angles of the vehicle model. This issue was resolved by utilizing the capabilities of ESC. Three variations of ESC were introduced in this paper, a conventional ESC with constant speed assumption, another conventional ESC with variable speed assumption, and an ESC for four-wheel motor drive vehicles that mitigates conventional ESC's speed reduction problem. ESC was designed using the 7-DOF horizontal model which considers lateral, longitudinal, and yaw dynamics, to control vehicle sideslip angle as well as the yaw rate and to improve vehicle lateral stability by using active rear-wheel braking system. The controllers developed were then applied to 14-DOF nonlinear full vehicle model, and the results were analyzed. It was observed that the integrated controller reduced not only the vehicle sideslip angle but also the yaw rate error. This has been achieved by the balanced vertical force distribution on each tire. The integration of ESC and AMC controllers was proven beneficial for the global safety of the full vehicle.

References

[1] Y. Shibahata, K. Shimada, T. Tomari. 1993. Improvement of Vehicle Maneuverability by Direct Yaw Moment Control. *Vehicle Systems Dynamics.* 22 (5):465-481

[2] I. Youn, W. Liang, E. Youn and M. Tomizuka. 2015. Attitude Motion Control of the Active Suspension System with Tracking Controller. *International Journal of Automation Technology.* Vol 16.

[3] A. Javadian. 2010. A New Optimum Strategy for ESC to Share Forces among Four Wheels. JIMEC'7, Amman –Jordan.

[4] I. Youn, J. Im, and M. Tomizuka. 2006. Level and Attitude Control of the Active Suspension System with Integral and Derivative Action. *Vehicle System Dynamics.* Vol. 44: 659-674.

[5] R. Zhou, A. Zolotas, and R. Goodall. 2011. Integrated Tilt with Active Lateral Secondary Suspension Control for High Speed Railway Vehicles. *Mechatronics.* Vol. 21: 1108-1122.

[6] J. Wang and S. Shen. 2008. Integrated vehicle ride and roll control via active suspensions. *Vehicle System Dynamics*. Vol. 46: 495-508.

[7] M. Lakehal-Ayat. 2002. An Improved Active Suspension Yaw Rate Control. 2002 American Control Conference, Anchorage, AK. Vol. 2: 863-868.

[8] T. Shim and C. Ghike. 2007. Understanding the limitations of different vehicle models for roll dynamics studies. *Vehicle System Dynamics.* Volume 45, Issue 3: 191-216.

[9] R. Rajamani. 2005. *Vehicle Dynamics and Control*.

[10] H. B. Pacejka. 1987. Tyre Modelling for Use in Vehicle Dynamics Studies. *Society of Automotive Engineers, Inc*.

[11] Society of Automotive Engineers, 1970. Vehicle dynamics terminology. *SAE paper j670e*.

Appendix A

Equations for the 25 states of 14-DOF nonlinear full vehicle model:

$$m\dot{u} = \sum\left(F_{xsi}\right) + mg\sin\theta - m\left(\omega_y w - \omega_z v\right) \tag{A1}$$

$$m\dot{v} = \sum\left(F_{ysi}\right) - mg\sin\phi\cos\theta - m\left(\omega_z u - \omega_x w\right) \tag{A2}$$

$$m\dot{w} = \sum(F_{zsi} + F_{dzi}) - mg\cos\phi\cos\theta - m\left(\omega_x v - \omega_y u\right) \tag{A3}$$

$$\dot{\theta} = \omega_y\cos\phi - \omega_z\sin\phi \tag{A4}$$

$$\dot{\phi} = \omega_x + \omega_y\sin\phi\tan\theta + \omega_z\tan\theta\cos\phi \tag{A5}$$

$$\dot{\psi} = \omega_y\frac{\sin\phi}{\cos\theta} + \omega_z\frac{\cos\phi}{\cos\theta} \tag{A6}$$

$$J_y\dot{\omega}_y = \sum_{i=1}^{4} M_{yi} - \left(F_{zs1} + F_{zs2}\right)c + \left(F_{zs3} + F_{zs4}\right)d \tag{A7}$$

$$J_x\dot{\omega}_x = \sum_{i=1}^{4} M_{xi} - \left(F_{zs1} + F_{zs4}\right)a + \left(F_{zs2} + F_{zs3}\right)b \tag{A8}$$

$$\begin{aligned} J_z\dot{\omega}_z &= \left(F_{xs1} + F_{xs4}\right)a - \left(F_{xs2} + F_{xs3}\right)b \\ &+ \left(F_{ys1} + F_{ys2}\right)c - \left(F_{ys3} + F_{ys4}\right)d \end{aligned} \tag{A9}$$

$$J_1\dot{\omega}_1 = -F_{xt1}r_1 + \tau_b \tag{A10}$$

$$J_2\dot{\omega}_2 = -F_{xt2}r_2 + \tau_b \tag{A11}$$

$$J_3\dot{\omega}_3 = -F_{xt3}r_3 + \tau_b \tag{A12}$$

$$J_4\dot{\omega}_4 = -F_{xt4}r_4 + \tau_b \tag{A13}$$

$$\dot{x}_{s1} = -w_{s1} + w_{u1} \tag{A14}$$

$$\dot{x}_{s2} = -w_{s2} + w_{u2} \tag{A15}$$

$$\dot{x}_{s3} = -w_{s3} + w_{u3} \tag{A16}$$

$$\dot{x}_{s4} = -w_{s4} + w_{u4} \tag{A17}$$

$$\dot{x}_{t1} = w_{g1} - (\cos\theta \cdot (w_{u1}\cos\phi + v_{u1}\sin\phi) - u_{u1}\sin\theta) \tag{A18}$$

$$\dot{x}_{t2} = w_{g2} - (\cos\theta \cdot (w_{u2}\cos\phi + v_{u2}\sin\phi) - u_{u2}\sin\theta) \tag{A19}$$

$$\dot{x}_{t3} = w_{g3} - (\cos\theta \cdot (w_{u3}\cos\phi + v_{u3}\sin\phi) - u_{u3}\sin\theta) \tag{A20}$$

$$\dot{x}_{t4} = w_{g4} - (\cos\theta \cdot (w_{u4}\cos\phi + v_{u4}\sin\phi) - u_{u4}\sin\theta) \tag{A21}$$

$$\begin{aligned} m_{u1}\dot{w}_{u1} &= \cos\phi \cdot (\cos\theta \cdot (F_{zg1} - m_{u1}g) + \sin\theta \cdot F_{xg1}) \\ &- \sin\phi \cdot F_{yg1} - F_{dz1} - F_{zs1} - m_{u1}(v_{u1} \cdot \omega_x - u_{u1} \cdot \omega_y) \end{aligned} \tag{A22}$$

$$\begin{aligned} m_{u2}\dot{w}_{u2} &= \cos\phi \cdot (\cos\theta \cdot (F_{zg2} - m_{u2}g) + \sin\theta \cdot F_{xg2}) \\ &- \sin\phi \cdot F_{yg2} - F_{dz2} - F_{zs2} - m_{u2}(v_{u2} \cdot \omega_x - u_{u2} \cdot \omega_y) \end{aligned} \tag{A23}$$

$$\begin{aligned} m_{u3}\dot{w}_{u3} &= \cos\phi \cdot (\cos\theta \cdot (F_{zg3} - m_{u3}g) + \sin\theta \cdot F_{xg3}) \\ &- \sin\phi \cdot F_{yg3} - F_{dz3} - F_{zs3} - m_{u3}(v_{u3} \cdot \omega_x - u_{u3} \cdot \omega_y) \end{aligned} \tag{A24}$$

$$\begin{aligned} m_{u4}\dot{w}_{u4} &= \cos\phi \cdot (\cos\theta \cdot (F_{zg4} - m_{u4}g) + \sin\theta \cdot F_{xg4}) \\ &- \sin\phi \cdot F_{yg4} - F_{dz4} - F_{zs4} - m_{u4}(v_{u4} \cdot \omega_x - u_{u4} \cdot \omega_y) \end{aligned} \tag{A25}$$

Appendix B

Derivation of *Variable Velocity* ESC Equation:

$$\rho_{yaw}\dot{\omega}_z + \rho_s\dot{\beta} = \rho_{yaw}\frac{a\left(F_{xg1}+F_{xg4}\right)-b\left(F_{xg2}+F_{xg3}\right)+c\left(F_{yg1}+F_{yg2}\right)-d\left(F_{yg3}+F_{yg4}\right)}{J_z}$$

$$+\rho_s\left(\frac{\sum_{i=1}^{4}F_{ygi}u-\sum_{i=1}^{4}F_{xgi}v}{m\left(u^2+v^2\right)}-\omega_z\right)$$

$$=\left(\frac{a\rho_{yaw}}{J_z}-\frac{\rho_s v}{mV^2}\right)\left(F_{xg1}+F_{xg4}\right)+\left(\frac{-b\rho_{yaw}}{J_z}-\frac{\rho_s v}{mV^2}\right)\left(F_{xg2}+F_{xg3}\right)$$

$$+\left(\frac{c\rho_{yaw}}{J_z}+\frac{\rho_s u}{mV^2}\right)\left(F_{yg1}+F_{yg2}\right)+\left(\frac{-d\rho_{yaw}}{J_z}+\frac{\rho_s u}{mV^2}\right)\left(F_{yg3}+F_{yg4}\right)-\rho_s\omega_z$$

$$=\left(\frac{a\rho_{yaw}}{J_z}-\frac{\rho_s v}{mV^2}\right)\left(F_{xt1}\cos\delta_1+F_{xt4}\cos\delta_4-F_{yt1}\sin\delta_1-F_{yt4}\sin\delta_4\right)$$

$$+\left(\frac{-b\rho_{yaw}}{J_z}-\frac{\rho_s v}{mV^2}\right)\left(F_{xt2}\cos\delta_2-F_{yt2}\sin\delta_2+F_{xt3}\cos\delta_3-F_{yt3}\sin\delta_3\right)$$

$$+\left(\frac{c\rho_{yaw}}{J_z}+\frac{\rho_s u}{mV^2}\right)\left(F_{xt1}\sin\delta_1+F_{yt1}\cos\delta_1+F_{xt2}\sin\delta_2+F_{yt2}\cos\delta_2\right)$$

$$+\left(\frac{-d\rho_{yaw}}{J_z}+\frac{\rho_s u}{mV^2}\right)\left(F_{xt3}\sin\delta_3+F_{yt3}\cos\delta_3+F_{xt4}\sin\delta_4+F_{yt4}\cos\delta_4\right)-\rho_s\omega_z$$

$$=F_{xt1}\left\{\cos\delta_1\left(\frac{a\rho_{yaw}}{J_z}-\frac{\rho_s v}{mV^2}\right)+\sin\delta_1\left(\frac{c\rho_{yaw}}{J_z}+\frac{\rho_s u}{mV^2}\right)\right\}$$

$$+F_{xt2}\left\{\cos\delta_2\left(\frac{-b\rho_{yaw}}{J_z}-\frac{\rho_s v}{mV^2}\right)+\sin\delta_2\left(\frac{c\rho_{yaw}}{J_z}+\frac{\rho_s u}{mV^2}\right)\right\}$$

$$+F_{xt3}\left\{\cos\delta_3\left(\frac{-b\rho_{yaw}}{J_z}-\frac{\rho_s v}{mV^2}\right)+\sin\delta_3\left(\frac{-d\rho_{yaw}}{J_z}+\frac{\rho_s u}{mV^2}\right)\right\}$$

$$+F_{xt4}\left\{\cos\delta_4\left(\frac{a\rho_{yaw}}{J_z}-\frac{\rho_s v}{mV^2}\right)+\sin\delta_4\left(\frac{-d\rho_{yaw}}{J_z}+\frac{\rho_s u}{mV^2}\right)\right\}$$

$$+F_{yt1}\left\{\cos\delta\left(\frac{c\rho_{yaw}}{J_z}+\frac{\rho_s u}{mV^2}\right)+\sin\delta_1\left(\frac{-a\rho_{yaw}}{J_z}+\frac{\rho_s v}{mV^2}\right)\right\}$$

$$+F_{yt2}\left\{\cos\delta_2\left(\frac{c\rho_{yaw}}{J_z}+\frac{\rho_s u}{mV^2}\right)+\sin\delta_2\left(\frac{b\rho_{yaw}}{J_z}+\frac{\rho_s v}{mV^2}\right)\right\}$$

$$+F_{yt3}\left\{\cos\delta_3\left(\frac{-d\rho_{yaw}}{J_z}+\frac{\rho_s u}{mV^2}\right)+\sin\delta_3\left(\frac{b\rho_{yaw}}{J_z}+\frac{\rho_s v}{mV^2}\right)\right\}$$

$$+F_{yt4}\left\{\cos\delta_4\left(\frac{-d\rho_{yaw}}{J_z}+\frac{\rho_s u}{mV^2}\right)+\sin\delta_4\left(\frac{-a\rho_{yaw}}{J_z}+\frac{\rho_s v}{mV^2}\right)\right\}-\rho_s\omega_z$$

$$
\begin{aligned}
&= F_{xt1}\left\{\cos\delta_1\left(\frac{a\rho_{yaw}}{J_z}-\frac{\rho_s v}{mV^2}\right)+\sin\delta_1\left(\frac{c\rho_{yaw}}{J_z}+\frac{\rho_s u}{mV^2}\right)\right\} \\
&+F_{xt2}\left\{\cos\delta_2\left(\frac{-b\rho_{yaw}}{J_z}-\frac{\rho_s v}{mV^2}\right)+\sin\delta_2\left(\frac{c\rho_{yaw}}{J_z}+\frac{\rho_s u}{mV^2}\right)\right\} \\
&+F_{xt3}\left(\frac{-b\rho_{yaw}}{J_z}-\frac{\rho_s v}{mV^2}\right)+F_{xt4}\left(\frac{a\rho_{yaw}}{J_z}-\frac{\rho_s v}{mV^2}\right) \\
&+F_{yt1}\left\{\cos\delta\left(\frac{c\rho_{yaw}}{J_z}+\frac{\rho_s u}{mV^2}\right)+\sin\delta_1\left(\frac{-a\rho_{yaw}}{J_z}+\frac{\rho_s v}{mV^2}\right)\right\} \\
&+F_{yt2}\left\{\cos\delta_2\left(\frac{c\rho_{yaw}}{J_z}+\frac{\rho_s u}{mV^2}\right)+\sin\delta_2\left(\frac{b\rho_{yaw}}{J_z}+\frac{\rho_s v}{mV^2}\right)\right\} \\
&+F_{yt3}\left(\frac{-d\rho_{yaw}}{J_z}+\frac{\rho_s u}{mV^2}\right)+F_{yt4}\left(\frac{-d\rho_{yaw}}{J_z}+\frac{\rho_s u}{mV^2}\right)-\rho_s\omega_z \\
&= \sum_{i=1}^{4}F_{xti}\kappa_{Fyti}+\sum_{i=1}^{4}F_{yti}\kappa_{Fyti} \\
&= \rho_{yaw}\dot{\omega}_{zd}-K_{ESC}\left(\rho_{yaw}\left(\omega_z-\omega_{zd}\right)+\rho_s\beta\right)
\end{aligned}
$$

where,

$$
\begin{aligned}
\kappa_{Fxt1} &= \frac{\rho_{yaw}}{J_z}(a\cos\delta_1+c\sin\delta_1)-\frac{\rho_s}{m\left(u^2+v^2\right)}(v\cos\delta_1-u\sin\delta_1) \\
\kappa_{Fxt2} &= \cos\delta_2\left(\frac{-b\rho_{yaw}}{J_z}-\frac{\rho_s v}{m\left(u^2+v^2\right)}\right)+\sin\delta_2\left(\frac{c\rho_{yaw}}{J_z}+\frac{\rho_s u}{m\left(u^2+v^2\right)}\right) \\
\kappa_{Fxt3} &= \frac{-b\rho_{yaw}}{J_z}-\frac{\rho_s v}{m\left(u^2+v^2\right)} \\
\kappa_{Fxt4} &= \frac{a\rho_{yaw}}{J_z}-\frac{\rho_s v}{m\left(u^2+v^2\right)} \\
\kappa_{Fyt1} &= \cos\delta\left(\frac{c\rho_{yaw}}{J_z}+\frac{\rho_s u}{m\left(u^2+v^2\right)}\right)+\sin\delta_1\left(\frac{-a\rho_{yaw}}{J_z}+\frac{\rho_s v}{m\left(u^2+v^2\right)}\right) \\
\kappa_{Fyt2} &= \cos\delta_2\left(\frac{c\rho_{yaw}}{J_z}+\frac{\rho_s u}{m\left(u^2+v^2\right)}\right)+\sin\delta_2\left(\frac{b\rho_{yaw}}{J_z}+\frac{\rho_s v}{m\left(u^2+v^2\right)}\right) \\
\kappa_{Fyt3} &= \frac{-d\rho_{yaw}}{J_z}+\frac{\rho_s u}{m\left(u^2+v^2\right)} \\
\kappa_{Fyt4} &= \frac{-d\rho_{yaw}}{J_z}+\frac{\rho_s u}{m\left(u^2+v^2\right)}
\end{aligned}
$$

Derivation of *Constant Velocity* ESC Equation:

$$\rho_{yaw}\dot{\omega}_z + \rho_s\dot{\beta} = \rho_{yaw}\frac{a\left(F_{xg1}+F_{xg4}\right)-b\left(F_{xg2}+F_{xg3}\right)+c\left(F_{yg1}+F_{yg2}\right)-d\left(F_{yg3}+F_{yg4}\right)}{J_z} + \rho_s\frac{\sum F_{yg_i}}{m_T u} - \omega_z$$

$$= \frac{a\rho_{yaw}}{J_z}\left(F_{xg1}+F_{xg4}\right) + \frac{-b\rho_{yaw}}{J_z}\left(F_{xg2}+F_{xg3}\right)$$

$$+\left(\frac{c\rho_{yaw}}{J_z}+\frac{\rho_s}{m_T u}\right)\left(F_{yg1}+F_{yg2}\right) + \left(\frac{-d\rho_{yaw}}{J_z}+\frac{\rho_s}{m_T u}\right)\left(F_{yg3}+F_{yg4}\right) - \rho_s\omega_z$$

$$= \frac{a\rho_{yaw}}{J_z}\left(F_{xt1}\cos\delta_1 + F_{xt4}\cos\delta_4 - F_{yt1}\sin\delta_1 - F_{yt4}\sin\delta_4\right)$$

$$+\frac{-b\rho_{yaw}}{J_z}\left(F_{xt2}\cos\delta_2 - F_{yt2}\sin\delta_2 + F_{xt3}\cos\delta_3 - F_{yt3}\sin\delta_3\right)$$

$$+\left(\frac{c\rho_{yaw}}{J_z}+\frac{\rho_s}{m_T u}\right)\left(F_{xt1}\sin\delta_1 + F_{yt1}\cos\delta_1 + F_{xt2}\sin\delta_2 + F_{yt2}\cos\delta_2\right)$$

$$+\left(\frac{-d\rho_{yaw}}{J_z}+\frac{\rho_s}{m_T u}\right)\left(F_{xt3}\sin\delta_3 + F_{yt3}\cos\delta_3 + F_{xt4}\sin\delta_4 + F_{yt4}\cos\delta_4\right) - \rho_s\omega_z$$

$$= F_{xt1}\left\{\cos\delta_1\frac{a\rho_{yaw}}{J_z} + \sin\delta_1\left(\frac{c\rho_{yaw}}{J_z}+\frac{\rho_s}{m_T u}\right)\right\}$$

$$+F_{xt2}\left\{\cos\delta_2\frac{-b\rho_{yaw}}{J_z} + \sin\delta_2\left(\frac{c\rho_{yaw}}{J_z}+\frac{\rho_s}{m_T u}\right)\right\}$$

$$+F_{xt3}\left\{\cos\delta_3\frac{-b\rho_{yaw}}{J_z} + \sin\delta_3\left(\frac{-d\rho_{yaw}}{J_z}+\frac{\rho_s}{m_T u}\right)\right\}$$

$$+F_{xt4}\left\{\cos\delta_4\frac{a\rho_{yaw}}{J_z} + \sin\delta_4\left(\frac{-d\rho_{yaw}}{J_z}+\frac{\rho_s}{m_T u}\right)\right\}$$

$$+F_{yt1}\left\{\cos\delta\left(\frac{c\rho_{yaw}}{J_z}+\frac{\rho_s}{m_T u}\right) + \sin\delta_1\frac{-a\rho_{yaw}}{J_z}\right\}$$

$$+F_{yt2}\left\{\cos\delta_2\left(\frac{c\rho_{yaw}}{J_z}+\frac{\rho_s}{m_T u}\right) + \sin\delta_2\frac{b\rho_{yaw}}{J_z}\right\}$$

$$+F_{yt3}\left\{\cos\delta_3\left(\frac{-d\rho_{yaw}}{J_z}+\frac{\rho_s}{m_T u}\right) + \sin\delta_3\frac{b\rho_{yaw}}{J_z}\right\}$$

$$+F_{yt4}\left\{\cos\delta_4\left(\frac{-d\rho_{yaw}}{J_z}+\frac{\rho_s}{m_T u}\right) + \sin\delta_4\frac{-a\rho_{yaw}}{J_z}\right\} - \rho_s\omega_z$$

$$
\begin{aligned}
&= F_{xt1}\left\{\cos\delta_1 \frac{a\rho_{yaw}}{J_z} + \sin\delta_1\left(\frac{c\rho_{yaw}}{J_z} + \frac{\rho_s}{m_T u}\right)\right\} \\
&+F_{xt2}\left\{\cos\delta_2 \frac{-b\rho_{yaw}}{J_z} + \sin\delta_2\left(\frac{c\rho_{yaw}}{J_z} + \frac{\rho_s}{m_T u}\right)\right\} \\
&+F_{xt3}\frac{-b\rho_{yaw}}{J_z} + F_{xt4}\frac{a\rho_{yaw}}{J_z} \\
&+F_{yt1}\left\{\cos\delta\left(\frac{c\rho_{yaw}}{J_z} + \frac{\rho_s}{m_T u}\right) + \sin\delta_1 \frac{-a\rho_{yaw}}{J_z}\right\} \\
&+F_{yt2}\left\{\cos\delta_2\left(\frac{c\rho_{yaw}}{J_z} + \frac{\rho_s}{m_T u}\right) + \sin\delta_2 \frac{b\rho_{yaw}}{J_z}\right\} \\
&+F_{yt3}\left(\frac{-d\rho_{yaw}}{J_z} + \frac{\rho_s}{m_T u}\right) + F_{yt4}\left(\frac{-d\rho_{yaw}}{J_z} + \frac{\rho_s}{m_T u}\right) - \rho_s\omega_z
\end{aligned}
$$

$$
= \sum_{i=1}^{4} F_{xti}\kappa_{Fyti} + \sum_{i=1}^{4} F_{yti}\kappa_{Fyti} = \rho_{yaw}\dot{\omega}_{zd} - K_{ESC}\left(\rho_{yaw}\left(\omega_z - \omega_{zd}\right) + \rho_s\beta\right)
$$

where,

$$
\begin{aligned}
\kappa_{Fxt1} &= \frac{\rho_{yaw}}{J_z}\left(a\cos\delta_1 + c\sin\delta_1\right) + \sin\delta_1\frac{\rho_s}{m_T u} \\
\kappa_{Fxt2} &= \frac{\rho_{yaw}}{J_z}\left(c\sin\delta_2 - b\cos\delta_2\right) + \sin\delta_2\frac{\rho_s}{m_T u} \\
\kappa_{Fxt3} &= \frac{-b\rho_{yaw}}{J_z} \\
\kappa_{Fxt4} &= \frac{a\rho_{yaw}}{J_z} \\
\kappa_{Fyt1} &= \frac{\rho_{yaw}}{J_z}\left(c\cos\delta - a\sin\delta_1\right) + \cos\delta_1\frac{\rho_s}{m_T u} \\
\kappa_{Fyt2} &= \frac{\rho_{yaw}}{J_z}\left(c\cos\delta_2 + b\sin\delta_2\right) + \cos\delta_2\frac{\rho_s}{m_T u} \\
\kappa_{Fyt3} &= \frac{-d\rho_{yaw}}{J_z} + \frac{\rho_s}{m_T u} \\
\kappa_{Fyt4} &= \frac{-d\rho_{yaw}}{J_z} + \frac{\rho_s}{m_T u}
\end{aligned}
$$

Appendix C

Nonzero element of $A_{1(17x17)}$ matrix is defined as follows.

$$a_{1,1} = -(b_1 + b_2 + b_3 + b_4) / m$$

$$a_{1,4} = (b_1 \cdot c + b_2 \cdot c - b_3 \cdot d - b_4 \cdot d) / m$$

$$a_{1,5} = (b_1 \cdot a - b_2 \cdot b - b_3 \cdot b + b_4 \cdot a) / m$$

$$a_{1,6} = k_1 / m \, , a_{1,7} = k_2 / m \, , a_{1,8} = k_3 / m \, , a_{1,9} = k_4 / m$$

$$a_{1,14} = b_1 / m \, , a_{1,15} = b_2 / m \, , a_{1,16} = b_3 / m \, , a_{1,17} = b_4 / m$$

$$a_{2,4} = 1 \, , a_{3,5} = 1$$

$$a_{4,1} = (c \cdot (b_1 + b_2) - d \cdot (b_3 + b_4)) / J_y$$

$$a_{4,4} = (-c \cdot (b_1 \cdot c + b_2 \cdot c) - d \cdot (b_3 \cdot d + b_4 \cdot d)) / J_y$$

$$a_{4,5} = (-c \cdot (b_1 \cdot a - b_2 \cdot b) + d \cdot (b_4 \cdot a - b_3 \cdot b)) / J_y$$

$$a_{4,6} = -c \cdot k_1 / J_y \, , a_{4,7} = -c \cdot k_2 / J_y \, , a_{4,8} = d \cdot k_3 / J_y \, , a_{4,9} = d \cdot k_4 / J_y$$

$$a_{4,14} = -b_1 \cdot c / J_y \, , a_{4,15} = -b_2 \cdot c / J_y \, , a_{4,16} = b_3 \cdot d / J_y \, , a_{4,17} = b_4 \cdot d / J_y$$

$$a_{5,1} = (a \cdot (b_1 + b_4) - b \cdot (b_2 + b_3)) / J_x$$

$$a_{5,4} = (-a \cdot (b_1 \cdot c - b_4 \cdot d) + b \cdot (b_2 \cdot c - b_3 \cdot d)) / J_x$$

$$a_{5,5} = (-a \cdot (b_1 \cdot a + b_4 \cdot a) - b \cdot (b_2 \cdot b + b_3 \cdot b)) / J_x$$

$$a_{5,6} = -a \cdot k_1 / J_x \, , a_{5,7} = b \cdot k_2 / J_x \, , a_{5,8} = b \cdot k_3 / J_x \, , a_{5,9} = -a \cdot k_4 / J_x$$

$$a_{5,14} = -b_1 \cdot a / J_x \, , a_{5,15} = b_2 \cdot b / J_x \, , a_{5,16} = b_3 \cdot b / J_x \, , a_{5,17} = -b_4 \cdot a / J_x$$

$$a_{6,1} = -1 \, , a_{6,4} = c \, , a_{6,5} = a \, , a_{6,14} = 1 \, , a_{7,1} = -1 \, , a_{7,4} = c \, , a_{7,5} = -b \, , a_{7,15} = 1$$

$$a_{8,1} = -1 \, , a_{8,4} = -d \, , a_{8,5} = -b \, , a_{8,16} = 1 \, , a_{9,1} = -1 \, , a_{9,4} = -d \, , a_{9,5} = a \, , a_{9,17} = 1$$

$a_{10,14} = 1$, $a_{11,15} = 1$, $a_{12,16} = 1$, $a_{13,17} = 1$

$a_{14,1} = b_1 / m_{u1}$, $a_{14,4} = -b_1 \cdot c / m_{u1}$, $a_{14,5} = -b_1 \cdot a / m_{u1}$

$a_{14,6} = -k_1 / m_{u1}$, $a_{14,10} = -k_{t1} / m_{u1}$, $a_{14,14} = -b_1 / m_{u1}$

$a_{15,1} = b_2 / m_{u2}$, $a_{15,4} = -b_2 \cdot c / m_{u2}$, $a_{15,5} = b_2 \cdot b / m_{u2}$

$a_{15,7} = -k_2 / m_{u2}$, $a_{15,11} = -k_{t2} / m_{u2}$, $a_{15,15} = -b_2 / m_{u2}$

$a_{16,1} = b_3 / m_{u3}$, $a_{16,4} = b_3 \cdot d / m_{u3}$, $a_{16,5} = b_3 \cdot b / m_{u3}$

$a_{16,8} = -k_3 / m_{u3}$, $a_{16,12} = -k_{t3} / m_{u3}$, $a_{16,16} = -b_3 / m_{u3}$

$a_{17,1} = b_4 / m_{u4}$, $a_{17,4} = b_4 \cdot d / m_{u4}$, $a_{17,5} = -b_4 \cdot a / m_{u4}$

$a_{17,9} = -k_4 / m_{u4}$, $a_{17,13} = -k_{t4} / m_{u4}$, $a_{17,17} = -b_4 / m_{u4}$

Nonzero element of $B_{1(17x4)}$ matrix is defined as follows.

$b_{1,i} = 1/m, i = 1 \sim 4$

$b_{4,1} = -c / J_y$, $b_{4,2} = -c / J_y$, $b_{4,3} = d / J_y$, $b_{4,4} = d / J_y$

$b_{5,1} = -a / J_x$, $b_{5,2} = b / J_x$, $b_{5,3} = b / J_x$, $b_{5,4} = -a / J_x$

$b_{14,1} = -1/m_{u1}$, $b_{15,2} = -1/m_{u2}$, $b_{16,3} = -1/m_{u3}$, $b_{17,4} = -1/m_{u4}$

Nonzero element of $D_{1(17x6)}$ matrix is defined as follows.

$d_{4,6} = 1/J_y$, $d_{5,5} = 1/J_x$

$d_{10,1} = 1$, $d_{11,2} = 1$, $d_{12,3} = 1$, $d_{13,4} = 1$

Element of $Q_{(17x17)}$ matrix is defined as follows.

$q_{i,j} = \rho_1 a_{1,i} a_{1,j} + \rho_2 a_{4,i} a_{4,j} + \rho_3 a_{5,i} a_{5,j}$

Specially,

$$q_{2,2} = \rho_1 a_{1,2} a_{1,2} + \rho_2 a_{4,2} a_{4,2} + \rho_3 a_{5,2} a_{5,2} + \rho_8$$

$$q_{3,3} = \rho_1 a_{1,3} a_{1,3} + \rho_2 a_{4,3} a_{4,3} + \rho_3 a_{5,3} a_{5,3} + \rho_9$$

$$q_{6,6} = \rho_1 a_{1,6} a_{1,6} + \rho_2 a_{4,6} a_{4,6} + \rho_3 a_{5,6} a_{5,6} + \rho_4$$

$$q_{7,7} = \rho_1 a_{1,7} a_{1,7} + \rho_2 a_{4,7} a_{4,7} + \rho_3 a_{5,7} a_{5,7} + \rho_5$$

$$q_{8,8} = \rho_1 a_{1,8} a_{1,8} + \rho_2 a_{4,8} a_{4,8} + \rho_3 a_{5,8} a_{5,8} + \rho_6$$

$$q_{9,9} = \rho_1 a_{1,9} a_{1,9} + \rho_2 a_{4,9} a_{4,9} + \rho_3 a_{5,9} a_{5,9} + \rho_7$$

$$q_{10,10} = \rho_1 a_{1,10} a_{1,10} + \rho_2 a_{4,10} a_{4,10} + \rho_3 a_{5,10} a_{5,10} + \rho_{10}$$

$$q_{11,11} = \rho_1 a_{1,11} a_{1,11} + \rho_2 a_{4,11} a_{4,11} + \rho_3 a_{5,11} a_{5,11} + \rho_{11}$$

$$q_{12,12} = \rho_1 a_{1,12} a_{1,12} + \rho_2 a_{4,12} a_{4,12} + \rho_3 a_{5,12} a_{5,12} + \rho_{12}$$

$$q_{13,13} = \rho_1 a_{1,13} a_{1,13} + \rho_2 a_{4,13} a_{4,13} + \rho_3 a_{5,13} a_{5,13} + \rho_{13}$$

where, a is an element of A matrix, i=1~17, j=1~17

N1$_{(17x4)}$ matrix is defined as follows.

$$n_{1_{i,j}} = \rho_1 a_{1,i} b_{1,j} + \rho_2 a_{4,i} b_{4,j} + \rho_3 a_{5,i} b_{5,j}$$

where, a and b are elements of A and B matrixes, i=1~17, j=1~4

N2$_{(17x6)}$ matrix is defined as follows.

$$n_{2_{i,j}} = \rho_1 a_{1,i} d_{1,j} + \rho_2 a_{4,i} d_{4,j} + \rho_3 a_{5,i} d_{5,j}$$

where, a and d are elements of A and D matrixes, i=1~17, j=1~6

$R_{(4x4)}$ matrix is defined as follows.

$$\begin{bmatrix} r_{1,1}+\rho_{14} & r_{1,2} & r_{1,3} & r_{1,4} \\ r_{2,1} & r_{2,2}+\rho_{15} & r_{2,3} & r_{2,4} \\ r_{3,1} & r_{3,2} & r_{3,3}+\rho_{16} & r_{3,4} \\ r_{4,1} & r_{4,2} & r_{4,3} & r_{4,4}+\rho_{17} \end{bmatrix}$$

where, $r_{i,j} = \rho_1 b_{1,i} b_{1,j} + \rho_2 b_{4,i} b_{4,j} + \rho_3 b_{5,i} b_{5,j}$, b is an element of B

$M1_{(6x4)}$ matrix is defined as follows.

$$m_{1_{i,j}} = \rho_1 d_{1,i} b_{1,j} + \rho_2 d_{4,i} b_{4,j} + \rho_3 d_{5,i} b_{5,j}$$

where, b and d are elements of B and D matrixes, i=1~6, j=1~4